ARTICLE

https://doi.org/10.1590/2317-4889202120200057

BJGEO
Brazilian Journal of Geology

Whole-rock trace element analyses via LA-ICP-MS in glasses produced by sodium borate flux fusion

Felipe Padilha Leitzke[1]*, Aline Celuppi Wegner[1], Carla Cristine Porcher[1], Natália Isabel Malüe Vieira[1], Jasper Berndt[2], Stephan Klemme[2], Rommulo Vieira Conceição[1]

Abstract

Trace elements provide crucial information about the origin and evolution of the Earth. One common issue regarding their analyses is the reduced analyte recovery during hot plate acid digestion for some geological samples. To overcome this, alkali fluxes (e.g., Lithium borate) have been used to produce an homogeneous synthetic glass that can be used then for both X-ray fluorescence (XRF) and laser ablation inductively coupled plasma mass spectrometry (LA-ICP-MS). In this sense, we developed a method for LA-ICP-MS whole rock trace element analyses in glasses prepared by mixing high-purity sodium tetraborate and rock powders at high-temperature. We selected six international reference materials including peridotite (JP-1), basalt (BRP-1), kimberlite (SARM-39), pyroxenite (NIM-P), diorite (DR-N) and andesite (JA-1). Glasses were produced in a fully automatic fusion machine with step heating. Run products analyses were carried out on a Thermo® Element2 SF-ICP-MS coupled to a New Wave Research® Nd:YAG (213 nm) laser ablation system and on a Thermo® Element XR ICP-MS coupled to an Analyte G2 (193 nm) LA system. Results show that glasses are homogeneous and there is good agreement (generally > 90%) between our data and literature values for most trace elements, including large ion lithophile elements (LILE), high-field strength elements (HFSE) and rare-earth elements (REE).

KEYWORDS: laser ablation inductively coupled plasma mass; trace elements; geochemistry.

INTRODUCTION

Despite their low abundance, trace elements provide crucial information about geochemical processes during the origin and evolution of the Earth and other planets (e.g., Kelemen *et al.* 1993, Münker 2010, White 2013). For example, trace elements have long been used to constrain tectonic settings and petrogenesis of a given geological unit (e.g., Pearce *et al.* 1984, Whalen *et al.* 1987), in mineral exploration and the origin of ore deposits (e.g., Pearce and Gale 1977, Hutchinson and McDonald 2008, Reich *et al.* 2016), or even to constrain large-scale planetary differentiation processes (e.g., Pfänder *et al.* 2007, Leitzke *et al.* 2017). For this reason, the high demand for trace elements analysis has led to a wide methodological/instrumental development in the last 10 to 20 years in geochemistry, promoting increasingly expressive analytical results in this area. For example, one of the most recent advances was to use laser ablation split stream analyses for measuring Sm-Nd, U-Pb or Hf isotopes together with trace elements content from the same ablated sample volume in a multi collector inductively coupled plasma mass spectrometer (ICP-MS) (e.g., Kylander-Clark *et al.* 2013, DesOrmeau *et al.* 2015, Fisher *et al.* 2020). However, one of the difficulties in the development of new techniques in multipurpose analytical facilities is, in particular, the issue of contamination, which can lead to a temporary or permanent damage to other analytical routines and procedural blanks in the geochemistry laboratory.

The analyses of trace elements in geological materials is mainly performed employing mass spectrometry, either with ionization through ICP-MS or emission of secondary ions, with the former being more cost effective than the latter (Jenner and Arevalo 2016). Sample introduction in the ICP-MS system can be via solution nebulization of a pre-dissolved rock powder or fused glass, or from a solid sample via laser ablation (Jackson *et al.* 1992, Fryer *et al.* 1995, Russo *et al.* 2013). Solution nebulization ICP-MS (SN-ICP-MS) requires prior acid digestion of the samples (e.g., Taylor *et al.* 2002, Pinto *et al.* 2012) and has lower detection limits mainly due to the higher volume of material (mg level) and efficiency of ionization compared to laser ablation. However, reliability of SN-ICP-MS results is affected by incomplete digestion of samples that have minerals resistant to acid attack (e.g., zircon, monazite or rutile), as well as precipitation and adsorption during preparation, storage and data acquisition (Potts 1992, Eggins 2003). There are some alternatives to overcome these issues. The first is the use of analytical techniques that do not require sample digestion such as Spark Source Mass Spectrometry (SSMS), Secondary Ion Mass Spectrometry (SIMS) or instrumental neutron activation

[1]Instituto de Geociências, Universidade Federal do Rio Grande do Sul – Porto Alegre (RS), Brazil. E-mails: felipe.leitzke@ufrgs.br, celuppi@gmail.com, carla.porcher@ufrgs.br, natimalue@gmail.com, rommulo.conceicao@ufrgs.br, jberndt@uni-muenster.de

[2]Institut für Mineralogie, Universität Münster – Münster, Germany. E-mail: stephan.klemme@uni-muenster.de

*Corresponding author.

analysis (INAA) (e.g., Korotev 1996, Jochum *et al.* 2001). The second is to use silicate glass beads produced by mixing rock powder and alkali salts, which lower the melting point of the system, as already done for X-ray fluorescence (XRF) measurements, and subsequently dissolving them with acid or alkaline solutions (Ingamells 1970, Panteeva *et al.* 2003). Another approach, recently developed by Peters and Pettke (2017), uses laser ablation inductively coupled plasma mass spectrometry (LA-ICP-MS) in nanoparticulate pressed rock powders to acquire trace element concentration. By applying this method, the authors were able to produce homogeneous pressed powders and quantify all groups of trace elements in six geological reference materials (RM) with accuracy similar to solution nebulization ICP-MS.

Still, except for the pressed rock powder technique (Peters and Pettke 2017), methods to acquire whole-rock trace element data are time and resource consuming. One simple, rapid and cost-effective technique is to analyze glass beads by laser ablation ICP-MS, which is a technique that can determine accurately and precisely more than 60 elements in geological samples in less than one minute (Eggins 2003, Jenner and O'Neill 2012). With this method, Eggins (2003) summarized the four main advantages LA-ICP-MS analyses of geological materials produced via alkali flux fusion:

- possibility of coupling trace element analyses with XRF major element analyses;
- less time and resource consuming compared to conventional solution nebulization;
- simple spectral acquisition;
- more reliable sample digestion and consequently less uncertainty on analyte recovery.

Most of the studies that perform LA-ICP-MS trace analyses on glasses produced via alkali fusion use Lithium borate as flux material (Nesbitt *et al.* 1997, Ødegård and Hamester 1997, Günther *et al.* 2001, Eggins 2003), since this is the standard procedure for XRF. Lithium borate is used instead of Na-borate in XRF analyses because the latter is an element of interest in whole-rock major element composition. Nevertheless, applications of Lithium isotope geochemistry have increased recently (Tomascak *et al.* 2012). Moreover, ^{7}Li is one of the masses used for ICP-MS tuning, and there is a great interest in Li content of minerals and rocks for petrology and geochemistry, which makes the introduction of a large amount of Li into the ICP-MS system during laser ablation a problem in geochemical laboratories due to contamination and increase in background signals. One alternative is to produce these glasses employing sodium tetraborate ($Na_2B_4O_7{\cdot}10H_2O$), which is also less expensive than Lithium borate and readily available in most geochemistry laboratories. Therefore, this study aimed to present the evaluation of a rapid method for precisely and accurately determining whole-rock trace element content using LA-ICP-MS on glass beads produced by mixing high-purity sodium tetraborate and rock powders at high-temperature. Among the dataset of 27 trace elements chosen to be analyzed are the most relevant for geochemical applications, i.e., Sc, V, Cr, Ni, Cu, Zn, Rb, Sr, Y, Zr, Nb, Ba, La, Ce, Pr, Nd, Sm, Eu, Gd, Dy, Ho, Er, Yb, Lu, Hf, Ta, Th and U.

METHODS AND ANALYTICAL TECHNIQUES

Sample selection and glass production

For this study, we selected a set of six standard RM including one andesite (JA-1, Hakone Volcano, Geological Survey of Japan), one peridotite (JP-1, Geological Survey of Japan), one pyroxenite (NIM-P, Bushveld Complex, Mintek South Africa), one kimberlite (SARM39, Kimberley Mine, Mintek South Africa), one diorite (DR-N, Rocher de Neuntelstein, Centre de Recherches Pétrographiques et Géochimiques (CRPG), Vandœuvre-lès-Nancy, France), and one basalt (Ribeirão Preto, Instituto de Geociências, UNICAMP/Brazil). These certified RM comprise a large compositional range observed in nature, with SiO_2 contents from 33 to 65 wt.%, and all samples are well described in the literature and geochemical databases (e.g., GeoReM) (Jochum *et al.* 2005b). This enables not only direct comparison and validation of the developed method but also the use of these samples as future matrix-match external RM for LA-ICP-MS analyses. Glasses were produced in a fully automatic PanAnalytical® Eagon 2 fusion machine following a standard procedure used for XRF analyses, as described below. A 7:1 ratio of sodium tetraborate decahydrate ($Na_2B_4O_7{\cdot}10H_2O$) flux (7 g) was mixed with the rock powder (1 g) and placed in a 95% Pt – 5% Au crucible (melting point between 1,675 and 1,745°C) in the furnace. The true dilution ratio, after melting, however, is likely to lie around 3.79 to one, since almost half of the mass comprising water will evaporate during the glass production. The risk of using a flux that has almost half of it as water is that it such a large volume of gas can boil and blow out during the melting stage causing damage to the Pt ware or to the furnace. Because of that, we slowly heated the crucible from room temperature to the desired melting temperature (1,050°C), in order to release all water at a slow and constant rate and prevent that the mixture could be blown out of the crucible during glass production. The choice for 95% Pt – 5% Au alloy is widely used for crucibles when producing silicate glasses via flux fusion for XRF analyses because the gold content reduces the wetting so that the glass can be easily removed after solidification without leaving residues. High-purity Merck® sodium tetraborate decahydrate (> 99.5%) was chosen to avoid contamination of sample rock powders in the mixing stage. A droplet of Ammonium iodide was added to the mixture before each melting stage to additionally prevent that the glass would stick to the crucible wall. In order to test if the crucible has been previously contaminated by trace elements in prior fusion processes, one of our samples (JA-1) was duplicated, by melting it with an "old" crucible, which was already in use routinely in the XRF laboratory and the other with a brand new one, which was the same used for the rest of our samples. Temperature was raised to 1,050°C and sample was stirred for 13 minutes. The choice of this temperature is because it is well below the point where trace elements of interest become volatile, with the exception of Rb and Zn

(see Lodders 2003). After that, molten mixture was poured into a polished Pt plate with 32 mm diameter, forming a circular glass disc ca. 1.0 mm thick. Glasses were broken into small fragments and mounted in round 1" (25 mm ϕ) epoxy sections. Even though glasses already had a clean and plane surface, after mounting, they had to be re-polished to all be on the same height. Because of the hygroscopic characteristic of the sodium tetraborate glass, polishing was done with 0.3 micron alumina powder in ethanol and cleansed with kerosene due to the highly hygroscopic properties of the glass itself. Also, because the glass bead is highly hygroscopic, it is recommended that samples are kept in a desiccator to prevent formation of a white layer of hydrated borate on top of it (Fig. 1). Macroscopically, silicate glass beads were homogeneous and ranged in color from transparent to brown, green and black, while "blank" glass beads produced only from the $Na_2B_4O_7.10H_2O$ are transparent immediately after quenching, but almost instantaneously acquire humidity from the atmosphere and have a whitish layer of hydrated borate on the surface (Fig. 1, right). The more iron rich the rock powder was, the darker the produced glass was. Compiled major element composition of the RM and exact proportion of rock powder to flux is given in Table 1. The proportion between flux and sample is crucial for the method development and data reduction, as well as for future application of LA-ICP-MS trace element analyses in tandem with XRF whole rock composition, in order to evaluate the original amount of Na in the sample and the amount added by the $Na_2B_4O_7.10H_2O$.

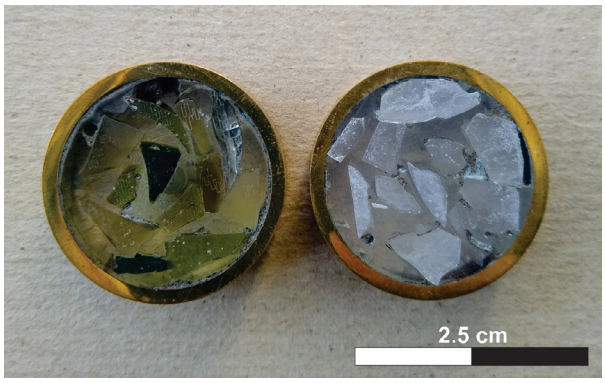

Figure 1. Glass beads produced in this study; sodium borate + rock powders (left) and only sodium borate, which was as necessary to control blank measurement and possible contamination from the flux (right).

LASER ABLATION INDUCTIVELY COUPLED PLASMA MASS SPECTROMETRY

LA-ICP-MS data was acquired at two different laboratories, the first series at the *Laboratório de Geologia Isotópica* (LGI), *Instituto de Geociências, Universidade Federal do Rio Grande do Sul* (UFRGS), Brazil, and the second at the *Institute für Mineralogie,* University of Münster, Germany. The ICP-MS and laser operating conditions are given in Table 2.

For the analyses at the LGI-UFRGS, a Thermo Fisher® Element 2 Sector Field ICP-MS was coupled to a New Wave Research® Nd:YAG deep UV (213 nm) laser ablation system (Fig. 2). Helium (compressed, 99.5 – 100% pure, White Martins/Praxair Inc., Rio de Janeiro, Brazil) flow was increased slowly to a constant rate of 0.5 L min^{-1} flushing into the laser sample cell to minimize surface re-condensation and maximize transport (Eggins *et al.* 1998, Eggins 2003). An auxiliary flow of Ar (Argon Pure Liquid 99.9%, Air Products, Guaíba, Brazil) fixed at 0.86 L min^{-1} was combined with He as carrier

Table 1. Major element composition of standard reference materials and rock powder to flux proportion.

SRM	JA-1	JP-1	NIM-P	DR-N	SARM-39	BRP-1
Rock type	Andesite	Peridotite	Pyroxenite	Diorite	Kimberlite	Basalt
Location	Hakone (J)	Horoman (J)	Bushveld (SA)	Neuntelstein (F)	Kimberley (SA)	Ribeirão Preto (BR)
*Whole-rock (wt. %)**						
Na_2O	3.87	0.02	0.37	2.99	0.50	2.71
MgO	1.57	44.65	26.51	4.40	26.24	3.94
Al_2O_3	15.10	0.64	4.08	17.52	4.29	12.40
SiO_2	64.20	42.38	52.12	52.85	33.44	50.39
P_2O_5	0.16	0.00	0.03	0.25	1.46	0.63
K_2O	0.77	0.00	0.10	1.70	1.04	1.52
CaO	5.70	0.55	2.93	7.05	9.69	7.95
TiO_2	0.86	0.01	0.24	1.09	1.58	3.81
MnO	0.15	0.12	0.24	0.22	0.17	0.21
Fe_2O_{3t}	7.01	8.35	13.01	9.70	9.29	15.59
LOI	1.51	3.20	0.50	2.26	-	0.50
Total	100.90	99.92	100.13	100.03	87.70	99.65
Sample (g)	1.0057	1.0065	1.0161	1.0170	1.0074	0.9827
$Na_2B_4O_7 \cdot 10H_2O$ (g)	7.0118	7.0200	7.0227	7.0199	7.0217	6.9935

*Reference values available at the Geological and Environmental Reference Materials database (GeoReM); SRM: Standard Reference Material; J: Japan; SA: South Africa; F: France; BR: Brazil.

gas prior to reaching the ICP-MS. Preliminary tests showed that line scans (raster) worked more effectively and were less time-consuming than spots in regard to homogeneity of the ICP-MS laser signal on the glasses. Sensitivity was monitored by ablation of the NIST-612 glass and maximized to always keep oxygen production rate below 0.1%, monitored by the formation of ThO^{+}. Line scans were performed with 100 µm diameter, 20 Hz and 5 µm s^{-1}. Signal stability under these conditions was ca. 5% RSD or less over a period of 2 to 3 minutes. A take-up ablation time of 5 seconds on the sample/standard before starting the analysis in the ICP-MS was used to ensure that all the system is purged with the ablation gas and set with the mixture of sample and sample gas, guaranteeing that there is no "gap" time in the analysis. In total, ten points in each sample and blank were done and results are an average of them, and each line scan lasted for around 2 minutes.

The analysis protocol at the LGI-UFRGS involved measuring the NIST SRM 612 glass before and after each sample assuming linear drift of the machine, as well as subtraction of "gas" background (laser turned off) from all count rates

Table 2. Inductively coupled plasma mass spectrometry and laser operating conditions.

ICP-MS		**Laser ablation**	
Isotope Geology Laboratory (Institute of Geosciences, UFRGS, Brazil)			
Magnetic Sector Field ICP-MS	Element2 from Thermo Fischer Scientific®	Model	UP213 Nd:YAG New Wave
Forward Power	1300 W	Wavelength	213 nm
Reflected Power	3 W	Max. Output energy	100%
Cool Gas flow (Ar)	15 L/min	Pulse width	4 ns
Aux. Gas flow (Ar)	0.86 L/min	Energy density	100 mJ
Ablation Cell gas flow (He)	0.5 L/min	Focus	Fixed at sample surface
Injector	Injektor quartz ICP II Ø 1,75 mm	Repetition rate	20 Hz
Sample Cone	Ni with 1.15 mm orifice	Spot size	100 µm
Skimmer Cone	Ni with 0.6 mm orifice	Ablation cell	Ø 2.54 cm
Runs	3	Sample time	0,075 s
Passes	2	Sample per peak	35
Take-up time	5 s	Passes	1
Magnet masses	42.958; 54.938; 73.921; 138.906; 180.947; 235.043	Speed	5 µm/s
Dwell time	0.285 s	Sampling scheme	raster (line)
Mass Window	150		
Acquisition Mode	Escan		
LA-ICP-MS laboratory (Institute of Mineralogy, University of Münster, Germany)			
Magnetic Sector Field ICP-MS	Element XR from Thermo Fischer Scientific®	Model	Analyte G2, Photon Machines
Forward Power	1300 W	Wavelength	193 nm
Reflected Power	< 1 W	Max. Output energy	15 J/cm^2
Cool Gas flow (Ar)	16 L/min	Pulse width	4 ns
Aux. Gas flow rate (Ar)	0.8 L/min	Energy density	4 J/cm^2
Ablation Cell gas flow (He)	1 L/min	Focus	Fixed at sample surface
Injector	Injektor quartz ICP II Ø 1,75 mm	Repetition rate	5 Hz
Sample Cone	Jet type Ni sampling cone with 1.1 mm orifice	Spot size	35 µm
Skimmer Cone	X-type Ni skimmer cone with 0.8 mm orifice	Ablation cell	HelEx-2-volume cell
Runs	28	Sample time	0.002 s
Passes	1	Sample per peak	100
Take-up time	40 s	Sampling scheme	spot
Magnet masses	42.958;58.933;84.911; 132.905;174.940;232.038		
Dwell time	2.163 s		
Mass Window	10		
Acquisition Mode	Escan		

LA-ICP-MS: laser ablation inductively coupled plasma mass spectrometry.

obtained for each analyte. An additional step was done to produce a background reference value for the borate fusion flux. A total of eleven borate discs produced by melting 8 g of $Na_2B_4O_7.10H_2O$ were also measured as unknown samples. The following isotopes were monitored during analyses in low resolution: ^{51}V, ^{52}Cr, ^{53}Cr, ^{60}Ni, ^{62}Ni, ^{63}Cu, ^{65}Cu, ^{66}Zn, ^{68}Zn, ^{85}Rb, ^{88}Sr, ^{89}Y, ^{90}Zr, ^{91}Zr, ^{92}Zr, ^{93}Nb, ^{137}Ba, ^{138}Ba, ^{139}La, ^{140}Ce, ^{142}Ce, ^{141}Pr, ^{142}Nd, ^{146}Nd, ^{150}Nd, ^{147}Sm, ^{152}Sm, ^{154}Sm, ^{153}Eu, ^{157}Gd, ^{160}Gd, ^{161}Dy, ^{163}Dy, ^{165}Ho, ^{166}Er, ^{168}Er, ^{170}Er, ^{172}Yb, ^{174}Yb, ^{175}Lu, ^{174}Hf, ^{178}Hf, ^{180}Hf, ^{181}Ta, ^{232}Th, ^{235}U, ^{238}U. Albeit not all of them yielded meaningful results, no correction for interfering isobaric or molecular species (e.g., $^{11}B^{40}Ar$ or $^{7}B^{36}Ar$) was done, and we chose to use only isotopes that are not prone to significant interferences (see Tab. 3 for selected masses) and keep oxygen production rate as low as possible (e.g., Eggins 2003). As seen from the list of analytes, special attention was given to refractory lithophile elements (Lodders 2003, Palme and O'Neill 2014), such as the large ion lithophile elements (LILE — e.g., Ba, Sr), high-field strength elements (HFSE — e.g., Zr, Hf, Ti), and rare-earth elements (REE — e.g., La, Ce, Eu, Lu), because they are not prone to volatilization to the atmosphere or diffusion to the crucible during rock powder melting. Data reduction was performed employing in-house spreadsheets which apply the method described in Longerich *et al.* (1996) and are detailed in section "Calibration strategy and data reduction". Both NIST-610 and NIST-612 glasses were used as external standards in this study, and ^{43}Ca as internal standard. The rationale of using two external standards was to check for measurement accuracy by using at each time either one or another as external standard and unknown and vice-versa. When this was done, values obtained for both NIST-610/612 do not deviate more than 5% of the preferred values reported by Jochum *et al.* (2011).

In order to verify the accuracy and precision of our results at the LGI-UFRGS, trace element concentrations of the glass pellets were also determined via LA-ICP-MS at the *Institut für Mineralogie* in Münster, Germany. Sample ablation was performed with a pulsed 193 nm ArF excimer laser (Analyte G2, Photon Machines). A spot size of 35 µm, repetition rate of 5 Hz and energy of ~3–4 J/cm^2 were chosen and elemental analysis carried out with an Element XR mass spectrometer (ThermoFisher Scientific). Forward power was 1300 W and reflected power < 1 W, gas flow rates were about 1 L/min for He (carrier gas of ablated material), 0.8 and 1 L/min for the Ar-auxiliary and sample gas, respectively. Before starting analysis, the system has been tuned on a NIST-612 reference glass measuring ^{139}La, ^{232}Th and $^{232}Th^{16}O$ to get stable signals and high sensitivity, as well as low oxide production rates ($^{232}Th^{16}O/^{232}Th < 0.1\%$). A total of 32 masses were monitored, including ^{7}Li, ^{29}Si, ^{43}Ca, ^{51}V, ^{53}Cr, ^{55}Mn, ^{59}Co, ^{60}Ni, ^{61}Ni, ^{63}Cu, ^{66}Zn, ^{69}Ga, ^{72}Ge, ^{73}Ge, ^{85}Rb, ^{88}Sr, ^{89}Y, ^{90}Zr, ^{93}Nb, ^{118}Sn, ^{121}Sb, ^{133}Cs, ^{137}Ba, ^{139}La, ^{140}Ce, ^{141}Pr, ^{146}Nd, ^{147}Sm, ^{153}Eu, ^{157}Gd, ^{159}Tb, ^{163}Dy, ^{165}Ho, ^{166}Er, ^{169}Tm, ^{172}Yb, ^{175}Lu, ^{178}Hf, ^{181}Ta, ^{182}W, ^{208}Pb, ^{232}Th and ^{238}U. External and internal standard were the NIST-612 and ^{43}Ca, respectively. Overall time of a single analysis was 75 s (20 s for background, 40 s for peak after switching on the laser, and 15 s of washout time). Concentrations of measured elements were calculated using the Glitter software (Griffin *et al.* 2008, Van Achterbergh *et al.* 2001). Standard reference glasses BHVO2-G and BIR1-G were analyzed as monitor for precision and accuracy. Obtained results match the published range of concentrations given in the GeoReM database and do not deviate more than 5% from the preferred values (Jochum *et al.* 2005b).

Limits of detection and sensitivity on LA-ICP-MS analyses are individual for each analyte mass, being a function of ionization efficiency, mass, concentration and amount of material extracted from the sample and introduced in the mass spectrometer (Longerich *et al.* 1996). Sensitivity can be monitored via NIST SRM 612 average measurements (Tab. 3 and Fig. 3). In order to quantify the limit of detection for each mass, it is necessary to measure several samples with no analyte, which is normally done by acquiring data only with the gas flow to the ICP-MS, without firing the laser, i.e., equivalent to the

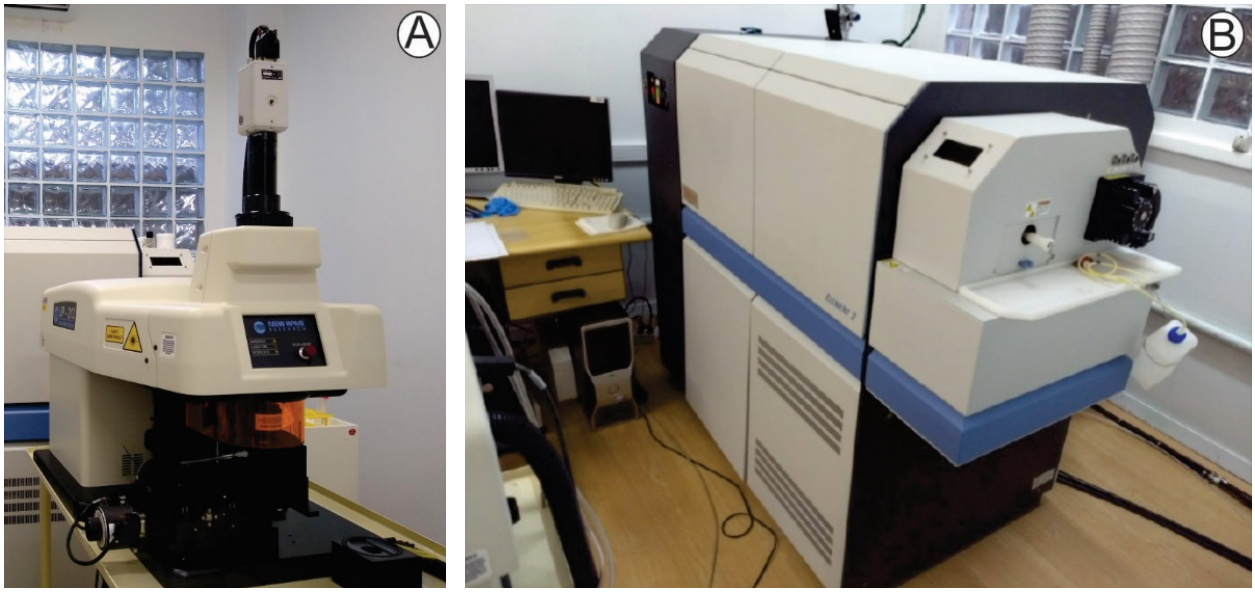

Figure 2. Laser ablation inductively coupled plasma mass spectrometry (LA-ICP-MS) apparatus used in this study; (A) New Wave Research® Nd:YAG deep UV (213 nm) laser ablation system; (B) Thermo Fisher® Element 2 Sector Field ICP-MS.

machine background (e.g., Longerich 2008). In addition, in the case of our study, we need to add the count rates measured on only borate discs that were produced without mixing with rock powders. Machine background is normally extremely low in LA-ICP-MS, especially for heavy analytes, with only a few counts per second. Therefore, to avoid dealing with the non-gaussian distribution of the background values when there are only a few measurements, Poisson counting statistics are applied, and the detection limit (DL) for each analyte (x) is determined by the Equation 1 (Golitko 2016):

$$DL_X = \frac{3.29 \cdot \sqrt{\mu_{BGx}} \cdot {}^{1}/_{\sqrt{n}} + 2.71}{S_x \cdot DT_x} \quad (1)$$

In which:

μ_{BGx} = mean value in counts per second of all background measurements;

DT = the dwell time;

n = the number of background measurements;

S_x = the sensitivity, i.e., the signal detected per unit of concentration.

In our case, we have two background values that need to be removed, and, hence, two possible DL. The first is the one calculated based solely on the Ar and He gas flow, and the second based on our measurement of eleven borate discs that were melted without sample mixture. The sum of both is the real analytical background when applying our method. By applying Equation 1, we obtain DL values ranging from the lowest value of 0.0009 µg/g for Ho to the highest of 2.8 µg/g for V (Tab. 3 and Fig. 3). Note that for some elements (Ni, Cu, Zn, V, Ba and Th) the background measured by ablating the sodium tetraborate discs, instead of only gas, increases, resulting in higher values of DL (Tab. 3), which indicates that these elements are present as impurities in the powder,

Table 3. Analyte elements and isotopes, NIST SRM 612 preferred values, and observed sensitivities and calculated detection limits for LA-ICP-MS analysis of Borax fused glasses.

Element	Selected mass	NIST SRM 612* (µg g-1)	Avg. Sensitivity (cps per µg g^{-1})	Background DL (µg g^{-1})	BG + Sodium borate DL (µg g^{-1})
V	**51**	**38.8**	**26,762**	**0.02**	**2.8**
Cr	53	36.4	2,659	0.7	0.7
Ni	**60**	**38.8**	**7,630**	**0.2**	**1.8**
Cu	**65**	**37.8**	**59,858**	**0.002**	**0.8**
Zn	**66**	**39.1**	**13,026**	**0.05**	**1.2**
Rb	85	31.4	29,753	0.04	0.05
Sr	88	78.4	29,153	0.1	0.1
Y	89	38.3	26,882	0.003	0.003
Zr	90	37.9	12,489	0.007	0.008
Nb	93	38.9	22,664	0.006	0.007
Ba	**137**	**39.3**	**4,646**	**0.02**	**0.3**
La	139	36.0	31,491	0.002	0.002
Ce	140	38.4	34,364	0.001	0.01
Pr	141	37.9	42,577	0.003	0.003
Nd	146	35.5	7,105	0.005	0.005
Sm	147	37.7	5,956	0.001	0.002
Eu	153	35.6	23,085	0.001	0.001
Gd	157	37.3	5,736	0.006	0.006
Dy	163	35.5	8,791	0.004	0.006
Ho	165	38.3	33,699	0.0006	0.0009
Er	166	38.0	10,910	0.006	0.006
Yb	172	39.2	7,144	0.008	0.008
Lu	175	37.0	31,678	0.001	0.001
Hf	178	36.7	11,119	0.001	0.001
Ta	181	37.6	32,781	0.001	0.001
Th	**232**	**37.8**	**29,674**	**0.0002**	**0.001**
U	238	37.4	41,465	0.003	0.003

*Preferred values reported by Jochum *et al.* (2011). For laser ablation inductively coupled plasma mass spectrometry (LA-ICP-MS) settings and analytical parameters see text and Table 2. Sensitivity is based on observed count rates during analysis of NIST SRM 612 glass. Detection limit take into account the average countrate for 11 sodium borate discs produced in a similar fashion to the samples, i.e., the dilution factor of 7:1 (total approx. 8 g).
BG: background, DL: detection limit.

possibly contaminating the sample by a significant amount. This exacerbates the importance of producing and analyzing systematically glasses with only flux and no sample, given that these values have to be subtracted from the count rates of the samples to provide a precise and accurate result.

Calibration strategy and data reduction

Differences in ablation yield a common issue with LA-ICP-MS analyses, i.e., the extent of material transported from the sample to the ICP-MS during the acquisition time. They can arise not only from changes in ablation conditions (e.g., spot size, frequency and energy) but also from distinct physicochemical properties of materials that can absorb a particular laser wavelength weakly or strongly causing extensive variation on the ablation yield (e.g., Jackson 2008). Moreover, differences in the ionization potential, melting and boiling point, and, in turn, volatility of the chemical elements, can cause elemental fractionation between vapor and the solid phase during ablation, despite otherwise ideal conditions (e.g., Fryer *et al.* 1995, Outridge *et al.* 1998, Chen 1999, Kuhn and Günther 2004). To overcome any issues with the changes in the amount of material that is ablated, transported and ionized at the ICP-MS, a correction factor is applied by using internal standardization. In this study, the calibration and quantification of the LA-ICP-MS data was performed by combining periodically (at the beginning and end) the ablation of an external standard (NIST-610/612 glasses) to an internal standard (^{43}Ca), which is an element of known concentration in

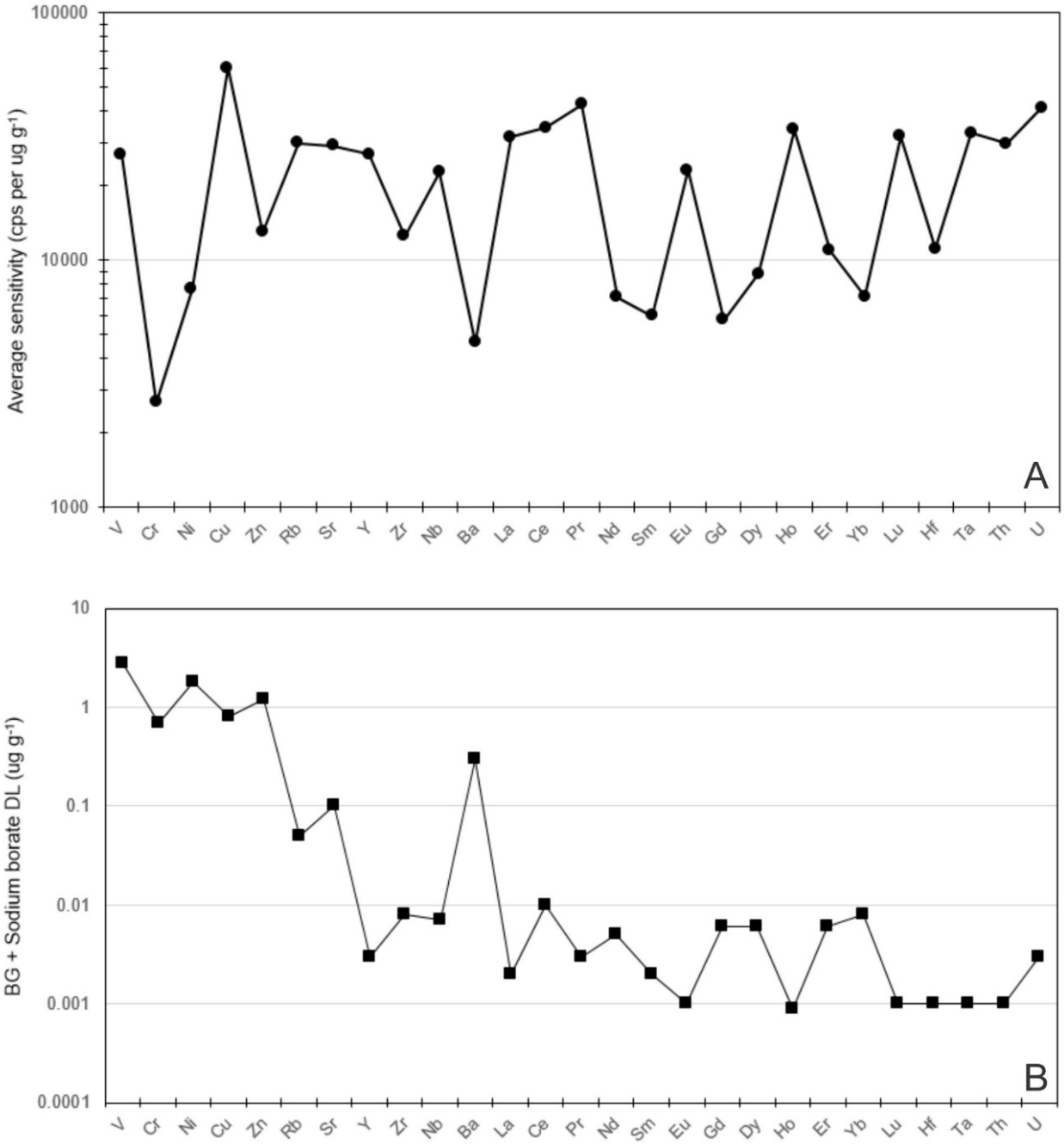

BG: background, DL: detection limit.

Figure 3. (A) Average sensitivity obtained for each measured element during ablation of NIST SRM 612 silicate glass (laser @ 100 µm and 20 Hz) at the LGI-UFRGS (Brazil); (B) Detection limit obtained by the sum of background measurements in 11 blank sodium borate glass and machine background (only with Ar and he gas flow).

the sample and standard (e.g., Jackson 2008). This procedure has been recognized to provide accurate analyses for many trace elements (Jackson *et al.* 1992, Perkins *et al.* 1993, Eggins 2003, Wu *et al.* 2018). The choice of ^{43}Ca as internal standard fulfils the requirements established by Jackson (2008), since this element is homogeneously distributed individually in the samples, it is present in sufficient concentration for both determination via LA-ICP-MS and an independent method (in our case, EPMA-WDS) and has the same fractionation behavior as the analytes. Moreover, by using 100 μm and ^{43}Ca as internal standard, we avoided laser induced element fractionation (LIEF) that could be exacerbated by using a smaller spot size. Regarding LIEF, Jenner and Arevalo (2016) have shown that the use of ^{29}Si (which would be another option for these glasses) produces LIEF offset to systematically higher values in reference silicate glasses such as BCR-2G, VG-2 and NIST-612, something that is not observed when using ^{43}Ca as internal standard. When ^{43}Ca is used as internal standard to obtain trace element content in reference silicate glasses, LIEF patterns between Ca and other elements are comparable, eliminating the need for a correction factor (see Fig. 2 in Jenner and Arevalo 2016). The choice of the NIST 610 and 612 glasses as external standards is justified because they have been used routinely to calibrate LA-ICP-MS trace element analyses of several geological materials successfully, from strongly UV-absorbing materials (e.g., titanite) to colorless, weakly UV-absorbing materials, such as fluorite or silicate glasses (see Jackson *et al.* 1992, Jackson 2008). Throughout the analysis run, blank (background) values were recorded by flushing the carrier gas (He) into the ICP-MS, without firing the laser, and these values were discounted from the laser signal values. Internal standard normalized count rates were converted to concentrations using the count rates of spots carried out on the NIST 610 and 612 glasses as the external standard, using preferred values of Jochum *et al.* (2011), and the methodology of Longerich *et al.* (1996), which is represented by the Equation 2:

$$[C]_M^S = [C]_M^{ES} \cdot {(CR)_M^S}/{(CR)_M^{ES}} \cdot \left[{[C]_M^{IS}}/{(CR)_M^{IS}} \cdot {(CR)_{ES}^{IS}}/{[C]_{ES}^{IS}} \right] \quad (2)$$

Where:

$[C]$ = concentration;

S = sample;

M = mass (analyte);

(CR) = count rate;

IS = internal standard (in our study ^{43}Ca);

ES = external standard (in our study the NIST SRM 610 and 612 glasses).

RESULTS AND COMPARISON WITH LITERATURE REFERENCE VALUES

LA-ICP-MS average whole-rock concentration and uncertainty obtained for twenty-seven trace elements in six RM determined at the LGI-UFRGS are given in Table 4, as well as lower and upper limits of the reported values for the same RM in the literature extracted from the "Geological and Environmental Reference Materials database – GeoReM" (Jochum *et al.* 2005b) on its online version 27 (02/01/2020). Literature data on these RM was obtained by several other analytical methods, for example SIMS, isotope dilution thermal ionization mass spectrometry (ID-TIMS), and conventional acid digestion and SN-ICP-MS.

When our data are compared with minimum and maximum literature values, there is an overall agreement for V, Cr, LILE, REE, and HFSE, which are refractory lithophile elements under the conditions our glasses were produced (Fig. 4). Barium, Th, and V, although present in significant amount in the sodium tetraborate powder, which resulted in higher DL (Tab. 3), were correctly determined by subtracting procedural blanks. On the other hand, Ni, Cu, and Zn show values that are offset systematically to lower values when compared to the minimum reported in the literature (Fig. 3). This is expected, because nickel is well known to have a siderophile behavior, and it is likely that it diffused to the Pt-crucible during the melting process, depleting the sample in this element (e.g., Wang *et al.* 2020). This is also the case for Cu and Zn, which, despite of their chalcophile behavior, can also act as moderately siderophile elements (Siebert *et al.* 2011, Mahan *et al.* 2017, Wang *et al.* 2020). Relative standard deviation obtained in the analyses in this study is within those expected for LA-ICP-MS analyses in the literature (e.g., Eggins 2003), being around 5–10% for most materials, and reaching up to 25% for the basalt BRP-1 (Tab. 4). The exception is the peridotite JP-1, for which analyses were close to the detection limit and uncertainty rose up to ca. 50% of the mean value in some cases (e.g., Eu, Gd, Dy, Ta).

There are at least two ways to quantitatively check for data accuracy obtained in this study by comparing the variation of our data to those obtained in this study from literature reference values (RV), i.e., $|X_{LA\text{-}ICP\text{-}MS} - X_{RV}|$ (Eggins 2003). A first and simple one described in Korotev (1996) considers the maximum uncertainty (σ_{max}) as the larger of the uncertainties of the RV (σ_{RV}) and the LA-ICP-MS analysis ($\sigma_{LA\text{-}ICP\text{-}MS}$). A second and more sophisticated approach is described in Eggins (2003) and makes a pooled uncertainty estimate taking into account both σ_{RV} and $\sigma_{LA\text{-}ICP\text{-}MS}$ by applying the Equation 3:

$$\sigma_{pooled} = \left({1}/{\sqrt{2}}\right) \times \sqrt{(\sigma_{RV^2} + \sigma_{LA-ICP-MS^2})} \quad (3)$$

To facilitate data visualization, all literature RV, average, minimum and maximum are also compiled in Table 4. According to Eggins (2003), the test for agreement at the 95% confidence level is if $|X_{LA\text{-}ICP\text{-}MS} - X_{RV}| < 1.96 \times \sigma_{pooled}$. Note that, because not all standard RM have preferred values at the GeoReM (Jochum *et al.* 2005b), we used maximum and minimum literature values to obtain the uncertainty associated with the RV (Tab. 4). By applying Equation 3, trace element content of the andesite reference material JA-1 at the 95% confidence level are 92% within the RV, except for Cu, with our data at 22.8 ± 8.1 μg/g, while average RV range between 36.6 and 48 μg/g, and U, in which we measured 0.3 ± 0.02 μg/g and literature ranges from 0.31 to 0.39 μg/g. For the Peridotite (JP-1) around 80% of the whole budget of trace elements are within literature values, but there are some significant variation in

Cr, Pr, Yb, and Lu, besides Ni and Cu, which were already discussed above. Values of Chromium determined in this study for the peridotite sample is 5754 ± 471 µg/g, while the literature ranges from 15.7 to 3,300 µg/g. Literature RV for Chromium vary by more than two orders of magnitude (Jochum *et al.* 2005a). Therefore, we can suggest that the presence of relict Fe-Cr-spinel microcrysts, which are highly refractory (melting point above 1,600°C) and common for this type of rock, did not react or melted entirely during the glass production process, generating an heterogeneity in the glass. Regarding Yb and Lu, measured values for the peridotite sample in this study are 0.045 ± 0.011 and 0.010 ± 0.003 µg/g, respectively, higher by a few ng/g when compared to literature, with values that range from 0.018 to 0.022 µg/g (Yb) and 0.001 to 0.006 µg/g (Lu). This indicates that data quality for the JP-1 peridotite was affected by measuring close to the detection limit for these elements. The Bushveld pyroxenite (NIM-P) has more than 95% of the values measured within the literature RV, with the only exception being Zn. Diorite (DR-N) and basalt (BRP-1) samples have more than 90% of the trace elements within literature RV, being the exception Ni, Cu and Zn. The Kimberlite SARM-39 sample also shows offset values for Ni, Cu and Zn, in addition to Cr and Yb, and an overall agreement of 81% when compared to the literature. Chromium content measured in the SARM-39 sample is 1,016 ± 56 while literature values range from 1,204 to 1,360, which could also be explained by areas that are enriched in Fe-Cr spinel microcrysts that did not react during glass production. Ytterbium literature RV for SARM-39 range from 0.86 to 1.04 µg/g, while in this study we measured 0.76 ± 0.05 µg/g, which is 10 ng/g below.

If we exclude from the accuracy evaluation (Eq. 3) the siderophile and chalcophile elements analysed in our study (i.e., Cu, Zn and Ni), i.e., elements that show consistent offset values linked to migration and diffusion to the crucible, and consider mostly litophile refractory elements such as LILE, REE and HFSE, we achieve an agreement with literature RV of more than 95% of trace elements being correctly determined for all RM measured in this study, including 100% agreement for samples NIM-P (Pyroxenite), DR-N (Diorite) and BRP-1 (Basalt). Moreover, the accuracy of our method is similar to the obtained by Eggins (2003) when performing a LA-ICP-MS study on trace elements but using lithium borosilicate glasses, showing that the method described here is accurate and precise to determine most of the trace elements of interest from a whole-rock powder.

In order to verify the accuracy and precision of the measurements performed at the LGI-UFRGS, borosilicate glass beads from the RM used in this study were also double-checked by

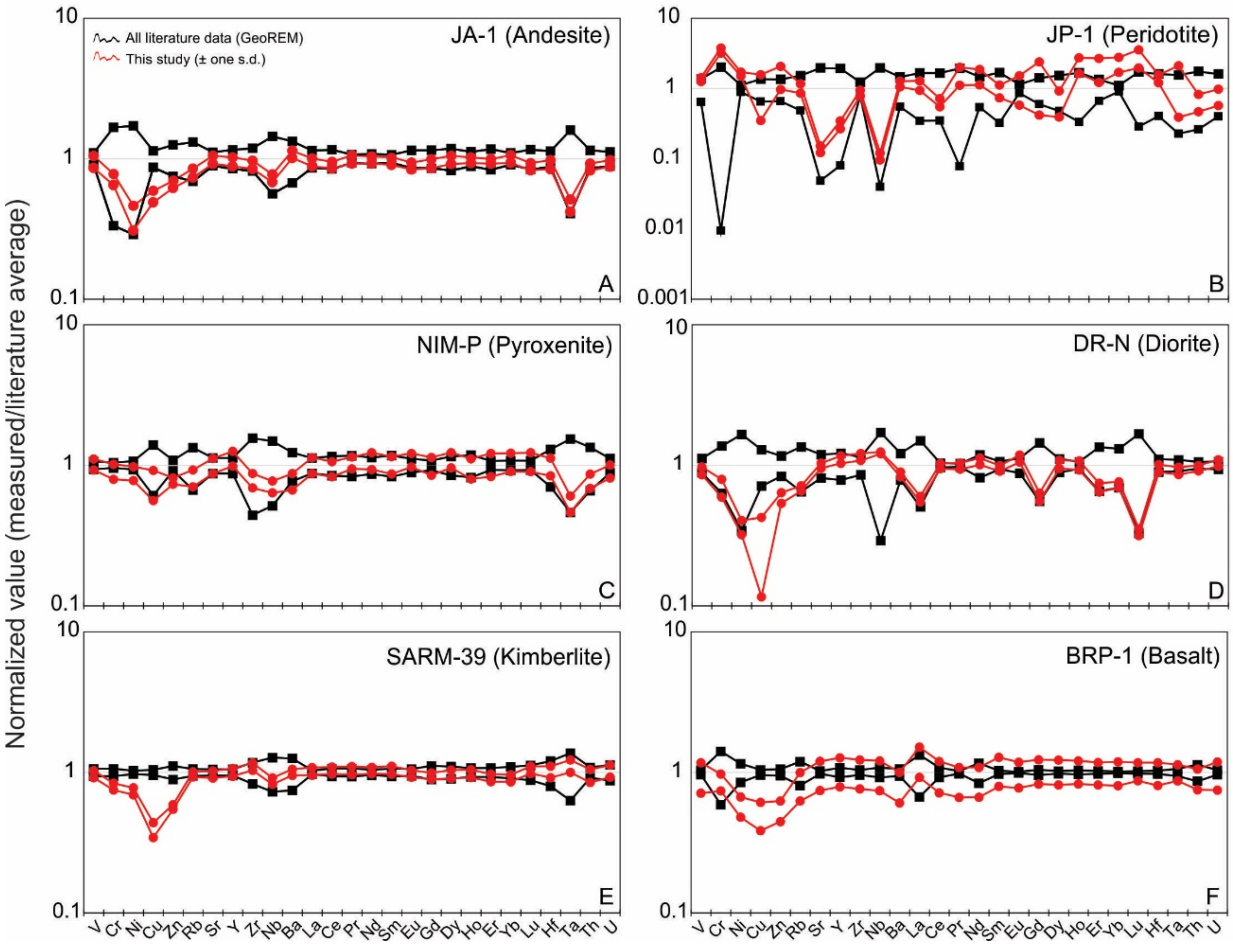

Figure 4. Laser ablation inductively coupled plasma mass spectrometry (LA-ICP-MS) trace element concentration of borosilicate glasses from geological reference materials obtained in this study (LGI-UFRGS) normalized to average literature values. Red lines indicate average values plus one standard deviation (minimum and maximum) normalized to the average literature, while black lines are minimum and maximum reported literature data (black lines). Literature data was extracted from the Geological and Environmental Reference Materials database, available at http://georem.mpch-mainz.gwdg.de/ (Jochum *et al.* 2005b).

Table 4. LA-ICP-MS trace element contents obtained on standard reference materials in this study (LGI-UFRGS, Brazil) and comparison with literature data (all in μg/g)*.

SRM	V	Cr	Ni	Cu	Zn	Rb	Sr	Y	Zr	Nb	Ba	La	Ce	Pr	Nd	Sm	Eu	Gd	Dy	Ho	Er	Yb	Lu	Hf	Ta	Th	U
JA-1 (Andesite)																											
Minimum (literature)	96.50	3.10	1.39	36.60	76.00	6.73	216.00	24.00	75.40	1.17	161.00	4.30	10.80	1.94	10.00	3.17	0.95	3.69	3.90	0.90	2.61	2.66	0.39	2.16	0.08	0.68	0.31
Maximum(literature)	117.00	15.50	8.23	48.00	127.00	12.80	270.00	32.70	109.32	3.00	318.00	5.70	14.80	2.22	11.70	3.61	1.27	4.96	5.58	1.14	3.66	3.22	0.54	2.80	0.31	0.91	0.39
Average (literature)	106.75	9.30	4.81	42.30	101.50	9.77	243.00	28.35	92.36	2.09	239.50	5.00	12.80	2.08	10.85	3.39	1.11	4.33	4.74	1.02	3.14	2.94	0.47	2.48	0.19	0.80	0.35
This study	101.75	6.63	1.85	22.81	66.66	7.73	239.13	26.97	83.75	1.21	257.37	4.71	11.52	2.06	10.61	3.27	0.98	3.99	4.65	1.00	3.00	2.92	0.41	2.25	0.09	0.69	0.30
SD	10.09	0.60	0.37	2.14	3.86	0.57	15.89	1.94	5.73	0.10	15.20	0.30	0.63	0.14	0.61	0.21	0.06	0.30	0.31	0.05	0.11	0.19	0.02	0.17	0.01	0.04	0.02
RSD (%)	9.92	9.03	20.03	9.39	5.79	7.35	6.65	7.21	6.84	7.84	5.91	6.36	5.44	6.82	5.71	6.37	5.65	7.48	6.63	4.61	3.76	6.34	5.89	7.40	10.24	5.58	5.96
JP-1 (Peridotite)																											
Minimum (literature)	17.50	15.70	2,201.00	3.46	29.90	0.26	0.50	0.06	4.02	0.03	8.70	0.021	0.042	0.001	0.027	0.008	0.003	0.006	0.010	0.001	0.010	0.018	0.001	0.080	0.020	0.009	0.010
Maximum(literature)	37.00	3,300.00	2,752.00	7.20	61.00	0.80	20.00	1.54	6.30	1.48	23.00	0.100	0.200	0.020	0.073	0.039	0.004	0.015	0.032	0.005	0.020	0.022	0.006	0.317	0.068	0.060	0.040
Average (literature)	27.25	1,657.85	2,476.50	5.33	45.45	0.53	10.25	0.80	5.16	0.76	15.85	0.060	0.121	0.010	0.050	0.023	0.004	0.011	0.021	0.003	0.015	0.020	0.004	0.199	0.044	0.035	0.025
This study	36.38	5,754.51	3,969.39	5.10	68.73	0.53	1.40	0.24	4.43	0.08	18.36	0.067	0.077	0.016	0.075	0.021	0.004	0.015	0.014	0.007	0.029	0.045	0.010	0.273	0.005	0.022	0.019
SD	2.35	471.83	261.14	3.24	24.91	0.08	0.15	0.03	0.41	0.01	1.71	0.010	0.010	0.005	0.018	0.004	0.002	0.006	0.006	0.002	0.011	0.011	0.003	0.035	0.003	0.006	0.005
RSD (%)	6.45	8.20	6.58	63.60	36.24	15.12	11.00	13.04	9.15	11.29	9.29	15.46	13.38	28.69	24.76	20.65	44.75	43.37	40.30	25.31	37.37	24.18	28.83	12.77	53.17	27.66	26.17
NIM-P (Pyroxenite)																											
Minimum (literature)	220	23,073	514	13.08	91.67	2.44	29.53	2.94	7.75	0.52	31.4	1.65	3.42	0.42	1.69	0.39	0.12	0.4	0.44	0.09	0.31	0.35	0.06	0.26	0.03	0.31	0.19
Maximum(literature)	250	25,163	588	29.9	108.83	4.88	38.08	3.79	27.36	1.5	50.23	2.12	4.7	0.59	2.22	0.55	0.15	0.47	0.6	0.13	0.36	0.41	0.07	0.48	0.1	0.63	0.24
Average (literature)	235	24,118	551	21.49	100.25	3.66	33.805	3.365	17.555	1.01	40.815	1.885	4.06	0.505	1.955	0.47	0.135	0.435	0.52	0.11	0.335	0.38	0.065	0.37	0.065	0.47	0.215
This study	239.054	21,814.6	482.979	15.878	77.400	2.981	33.620	3.772	13.709	0.511	31.396	1.891	3.832	0.427	2.112	0.474	0.148	0.432	0.569	0.135	0.342	0.463	0.079	0.363	0.035	0.364	0.195
SD	21.529	2,667.4	54.691	3.856	4.040	0.409	4.162	0.454	1.604	0.068	4.205	0.246	0.471	0.051	0.288	0.067	0.016	0.063	0.071	0.017	0.064	0.060	0.011	0.052	0.005	0.042	0.021
RSD (%)	9.01	12.23	11.32	24.29	5.22	13.72	12.38	12.05	11.70	13.38	13.39	13.03	12.30	11.99	13.63	14.19	11.06	14.61	12.41	12.77	18.77	12.99	13.48	14.32	13.32	11.59	10.71
DR-N (Diorite)																											
Minimum (literature)	178.27	27.00	11.00	46.00	127.11	67.60	299.80	18.85	107.36	4.00	305.95	17.79	43.40	5.40	16.23	4.74	1.41	4.50	3.93	0.89	2.45	2.30	0.34	2.89	0.54	4.53	1.49
Maximum(literature)	225.00	58.60	53.20	83.53	177.20	141.04	440.00	29.16	143.70	23.50	472.00	52.50	46.60	5.70	23.60	5.37	1.80	11.75	4.90	1.00	5.06	4.35	1.73	3.56	0.65	5.06	1.69
Average (literature)	201.64	42.80	32.10	64.77	152.16	104.32	369.90	24.01	125.53	13.75	388.98	35.15	45.00	5.55	19.92	5.06	1.61	8.13	4.42	0.95	3.75	3.32	1.04	3.23	0.60	4.80	1.59
This study	184.14	29.62	11.63	17.53	89.29	71.44	367.37	26.35	143.97	6.84	334.66	20.18	44.34	5.48	21.22	4.80	1.79	4.82	4.49	0.94	2.61	2.42	0.35	3.07	0.54	4.57	1.65
SD	11.75	4.32	1.35	10.03	7.76	3.06	15.49	1.59	8.43	0.26	13.61	0.93	1.90	0.28	1.18	0.22	0.11	0.32	0.30	0.07	0.19	0.12	0.02	0.19	0.03	0.20	0.09
RSD (%)	6.38	14.57	11.58	57.24	8.69	4.29	4.22	6.04	5.86	3.74	4.07	4.61	4.27	5.18	5.54	4.64	5.96	6.66	6.66	7.52	7.23	4.93	5.59	6.06	6.00	4.48	5.38
SARM-39 (Kimberlite)																											
Minimum (literature)	108.34	1,204.70	920.51	56.82	60.23	47.26	1,370.00	15.54	185.44	104.00	1,009.50	86.83	169.82	20.11	78.00	11.53	3.03	7.20	3.82	0.58	1.37	0.86	0.11	4.04	3.54	8.90	2.23
Maximum(literature)	122.34	1,360.00	973.00	61.91	75.19	52.87	1,514.30	17.20	262.62	182.16	1,702.80	92.52	192.51	22.89	85.49	13.06	3.38	9.01	4.67	0.67	1.59	1.04	0.14	6.10	7.70	10.54	2.88
Average (literature)	115.34	1,282.35	946.76	59.37	67.71	50.07	1,442.15	16.37	224.03	143.08	1,356.15	89.68	181.17	21.50	81.75	12.30	3.21	8.11	4.25	0.63	1.48	0.95	0.13	5.07	5.62	9.72	2.56
This study	112.20	1,016.47	695.11	23.19	38.44	48.44	1,395.17	16.41	246.57	124.13	1,359.45	91.31	187.04	22.17	84.38	12.78	3.14	7.63	4.12	0.55	1.30	0.76	0.11	5.13	6.25	9.21	2.62
SD	6.50	56.29	39.85	22.80	18.47	2.04	78.73	1.06	14.74	6.48	68.07	5.72	10.61	1.47	4.44	0.83	0.18	0.40	0.28	0.04	0.08	0.05	0.01	0.48	0.63	0.98	0.26
RSD (%)	5.79	5.54	5.73	98.28	48.04	4.22	5.64	6.46	5.98	5.22	5.01	6.27	5.67	6.65	5.26	6.49	5.70	5.20	6.90	7.06	6.35	6.52	6.87	9.35	10.08	10.61	9.83
BRP-1 (Basalt)																											
Minimum (literature)	376.00	7.10	19.30	149.00	132.00	29.10	490.00	37.80	294.00	27.70	513.00	21.00	90.50	11.70	50.40	10.60	3.33	9.44	8.17	1.50	4.07	3.39	0.48	7.69	1.78	3.58	0.77
Maximum(literature)	405.00	17.00	26.20	162.00	147.00	43.00	512.00	44.10	319.00	32.50	576.00	41.90	106.00	12.20	70.00	11.20	3.40	10.30	8.53	1.60	4.27	3.49	0.50	8.10	2.00	4.70	0.83
Average (literature)	390.50	12.05	22.75	155.50	139.50	36.05	501.00	40.95	306.50	30.10	544.50	31.45	98.25	11.95	60.20	10.90	3.37	9.87	8.35	1.55	4.17	3.44	0.49	7.90	1.89	4.14	0.80
This study	367.37	10.32	13.04	77.41	74.80	29.28	485.93	42.16	304.79	29.32	437.19	38.24	93.90	10.43	52.66	11.29	3.29	10.14	8.51	1.68	4.15	3.49	0.51	7.81	1.89	3.74	0.77
SD	89.78	1.42	2.14	17.62	12.50	6.73	114.05	9.84	71.22	7.03	107.33	9.31	23.67	2.51	12.65	2.64	0.68	1.99	1.70	0.30	0.75	0.66	0.07	1.45	0.25	0.63	0.18
RSD (%)	24.44	13.75	16.41	22.76	16.71	22.98	23.47	23.35	23.37	23.99	24.55	24.34	25.20	24.04	24.02	23.41	20.83	19.64	20.04	17.63	18.19	18.98	14.50	18.55	13.21	16.73	22.67

*Literature data compiled from the GeoReM database (Jochum *et al.* 2005a). Values in red are the ones that have no lower limit detected at the database, for which we assumed the lowest possible considering the least significant digit. Concentration values and uncertainties are rounded to the least significant digit, for the exact value used in the RSD calculation see the online version of the table; LA-ICP-MS: laser ablation inductively coupled plasma mass spectrometry. RSD: relative standard deviation; SD: standard deviation.

measuring trace element contents via LA-ICP-MS at the *Institut für Mineralogie* at the University of Münster (Germany), and results are given in Table 5. When our data are compared with minimum and maximum literature values from the GeoReM, the same overall agreement for V, Cr, LILE, REE, and HFSE is observed, as well as the depletion in Cu, Ni and Zn for some of the RM (Fig. 5).

Laser induced element fractionation is a common issue in LA-ICP-MS, already observed by the first published works that described this technique (e.g., Gray 1985, Fryer *et al.* 1995, Kroslakova and Günther 2007). For example, Fryer *et al.* (1995) showed that for chalcophile and volatile elements such as Cu, Zn, Cd, Ag, Sb, Tl and Pb, elemental fractionation relative to Ca occurs in the intensity of the signal as the ablation progresses deeper into the sample with time when measuring the NIST-610 RM. The factors responsible for the fractionation, however, are still not completely understood, being possible to be linked to the ablation process itself and aerosol transport, or during the vaporization, atomization, and ionization within the ICP (Kroslakova and Günther 2007). Regardless of the reason for the observed fractionation, it is widely accepted that it occurs due to the decrease in the laser pit size during progressive ablation (e.g., Eggins *et al.* 1998, Jenner and Arevalo 2016) and it could also be responsible for the divergence of our data from reported values in some cases. Whenever this occurs, the countrates for different elements and their ratio can vary progressively with time during the analyses, being not representative of the sample itself (e.g. Fryer *et al.* 1995, Eggins *et al.* 1998, Jackson 2008, Jenner and O'Neill 2012). This fractionation is controlled by external parameters such as wavelength, pulse duration; carrier gas composition and flow rates, as well as internal, such as optical and physicochemical properties of the sample substrate, geochemical behavior, element electronegativity, first ionization potential and condensation temperature (Jackson 2008, Russo *et al.* 2013, Arevalo 2014, Jenner and Arevalo 2016). Indeed, Jenner and Arevalo (2016) showed that there is an increase in element fractionation with decreasing volatility, and that siderophile and litophile elements are prone to negative fractionation when compared to ^{29}Si, for example, being necessary to apply a matrix correction to increase accuracy (Jenner and O'Neill 2012). However, when ^{43}Ca is used as internal standard, as in this study, even for non-matrix matching external standards, laser induced element fractionation is not significant, and no correction needs to be applied (Jenner and Arevalo 2016). In this sense, we can consider that even if element fractionation occurred during laser ablation of samples in this study, the choice of ^{43}Ca as internal standard was enough to account for its effect and provide reliable results, given that all analytes included here are classified as "routinely" analyzed in geological materials by LA-ICP-MS (Jenner and Arevalo 2016). It is important to point out that this indicates that the differences observed for Cu, Ni and Zn are likely due to their loss during glass production and not due to LIEF.

Heterogeneities of siderophile/chalcophile elements, such as Cu, Zn and Ni were also observed in MPI-DING and NIST RM in the literature, and their high affinity to form alloys with

Table 5. LA-ICP-MS trace element contents (µg/g) obtained on standard reference materials in this study (Institute für Mineralogie, University of Münster).

SRM	V	Cr	Ni	Cu	Zn	Rb	Sr	Y	Zr	Nb	Ba	La	Ce	Pr	Nd	Sm	Eu	Gd	Dy	Ho	Er	Yb	Lu	Hf	Ta	Th	U
JA-1 (*Andesite*)	114.24	bdl	bdl	22.62	78.68	10.14	262.06	27.67	80.15	1.42	292.21	5.19	13.66	2.18	10.49	3.57	1.14	4.39	4.52	1.14	3.16	3.16	0.472	2.56	0.11	0.76	0.34
SD	1.79	-	-	7.82	4.46	0.61	5.53	0.72	4.50	0.20	10.71	0.35	0.49	0.18	0.82	0.97	0.17	0.95	0.27	0.09	0.51	0.54	0.03	0.31	0.02	0.05	0.08
RSD (%)	1.57	-	-	34.58	5.67	6.00	2.11	2.60	5.62	13.89	3.67	6.74	3.59	8.47	7.82	27.08	14.70	21.65	6.04	8.27	16.03	17.16	5.83	12.06	18.60	7.05	24.64
JP-1 (*Peridotite*)	31.05	2,902.1	2,663.9	5.02	55.25	0.42	1.02	0.14	5.5	0.07	9.97	0.041	0.122	0.017	bdl	bdl	bdl	bdl	0.04	bdl	0.02	0.02	0.006	0.12	bdl	0.01	0.021
SD	2.82	50.18	165.59	1.35	9.72	0.10	0.29	0.03	0.70	0.04	1.40	0.018	0.027	0.005	-	-	-	-	0.015	-	0.010	0.009	0.001	0.076	-	0.004	0.004
RSD (%)	9.07	1.73	6.22	26.87	17.60	23.81	28.58	23.59	12.73	51.30	14.09	44.88	21.89	29.58	-	-	-	-	41.28	-	50.00	45.01	11.74	65.82	-	29.52	20.20
NIM-P (*Pyroxenite*)	233.14	25,330	578.5	24.11	102.18	2.51	36.31	3.15	11.03	0.581	35.37	2.01	4.02	0.5	1.93	0.43	0.17	0.46	0.55	0.12	0.323	0.41	0.069	0.37	0.034	0.34	0.24
SD	6.84	604.24	14.07	5.68	10.65	0.28	0.56	0.19	0.89	0.08	2.23	0.06	0.29	0.10	0.25	0.10	0.03	0.11	0.07	0.03	0.11	0.15	0.01	0.06	0.01	0.04	0.04
RSD (%)	2.94	2.39	2.43	23.56	10.42	11.22	1.55	6.16	8.04	12.98	6.30	2.78	7.34	20.86	13.07	25.01	19.40	24.69	12.57	27.54	34.66	37.78	17.23	15.47	29.41	10.36	16.66
DR-N (*Diorite*)	207.98	49.41	16.25	53.91	140.67	69.36	430.16	27.81	140.99	7.28	398.75	23.00	46.21	5.7	23.3	5.02	1.523	5.97	4.52	0.93	2.94	2.62	0.35	3.26	0.59	4.53	1.64
SD	10.35	4.35	7.05	6.42	21.39	3.15	23.05	0.98	6.11	0.69	17.18	0.77	2.09	0.38	1.80	0.98	0.30	0.89	1.24	0.12	0.71	0.63	0.07	0.65	0.07	0.39	0.19
RSD (%)	4.98	8.80	43.38	11.90	15.21	4.54	5.36	3.52	4.33	9.52	4.31	3.34	4.52	6.68	7.74	19.43	19.41	14.93	27.44	13.11	24.30	24.21	20.12	19.82	12.18	8.72	11.68
SARM-39 (*Kimberlite*)	106.81	1,325.9	952.55	61.43	55.7	52.36	1,431.7	15.56	246.71	137.6	1,267	90.5	183.8	20.19	79.37	11.9	3.01	7.96	3.96	0.65	1.49	0.96	0.13	5.5	6.59	8.9	2.34
SD	5.24	29.94	58.45	1.91	8.20	1.54	68.15	0.66	15.56	7.40	65.07	4.07	8.98	1.14	1.07	1.05	0.31	0.50	0.33	0.11	0.22	0.32	0.01	0.39	0.41	0.31	0.16
RSD (%)	4.90	2.26	6.14	3.12	14.72	2.93	4.76	4.26	6.31	5.38	5.14	4.49	4.89	5.67	1.35	8.85	10.44	6.31	8.33	17.28	14.81	33.21	5.80	7.09	6.22	3.47	6.83
BRP-1 (*Basalt*)	380.4	13	10.03	105.9	97.66	36.2	493.01	45.04	320.4	31.06	546.37	36.71	90.06	13.06	47.98	12.5	3.45	10.98	9.09	1.55	4.31	3.44	0.48	8.54	2.17	4.24	0.84
SD	11.44	2.96	1.90	10.62	8.35	1.09	5.49	1.32	16.61	2.01	11.43	1.88	4.74	0.60	3.86	0.46	0.29	1.55	0.53	0.27	0.74	0.53	0.02	0.52	0.15	0.26	0.12
RSD (%)	3.01	22.79	18.96	10.03	8.55	3.06	1.11	2.93	5.18	6.48	2.09	5.12	5.26	4.59	8.06	3.69	8.33	14.13	5.81	17.28	17.21	15.38	3.99	6.10	6.69	6.20	14.19

bdl: below detection limit; for LA-ICP-MS conditions see text. Concentration values and uncertainties are rounded to the least significant digit, for the exact value used in the RSD calculation see the online version of the table; LA-ICP-MS: laser ablation inductively coupled plasma mass spectrometry; RSD: relative standard deviation; SD: standard deviation.

Pt is also an issue to be considered as an interference factor in the determination of their contents (Jochum *et al.* 2005a, Kempenaers *et al.* 2003, Rocholl 1998). Copper, Zn and Ni can suffer fractionation due to their chalcophile/siderophile behavior, by preferential evaporation due the laser heat (Horn and von Blanckenburg 2007, Jochum *et al.* 2014), and also incomplete vaporization of large particles in the plasma source, due to inefficient ablation (Gaboardi and Humayun 2009). Another issue related to the incomplete vaporization is the influence of sample mass loaded by LA, which can influence the ratio of volatile chalcophile/siderophile elements (Jochum *et al.* 2012). Eggins *et al.* (1998) noted a systematic volatile element enrichment at shallower levels of ablation and refractory enrichment as the pit deepens into the samples. These authors analyzed ablation pit morphology and surface condensate material to interpret that element fractionation behavior reflects a change in the ablation processes itself, from photothermal to plasma dominated mechanisms, and the presence of surface deposits is reduced when the ablation is done under He when compared to Ar (Eggins *et al.* 1998).

In another study, Steenstra *et al.* (2019) summarized the main causes of elemental and isotopic fractionation during ablation and sample heating, ranging from sub-solidus reaction with phases formed close to the ablation pit (Kosler *et al.* 2005); non-congruent evaporation of volatile elements from the ablation pit (Hergenröder 2006); fractional condensation of the sample plume vapor during cooling after ablation (Eggins *et al.* 1998); and differential transport according the particle size and composition from the ablation cell to the ICP torch (Koch *et al.* 2002). In the same study, Steenstra *et al.* (2019) also pointed out that incomplete vaporization can result in higher count rates of more volatile elements (Guillong *et al.* 2003) and high loading of laser aerosols and their effect on plasma conditions can reduce signal intensities for volatile elements compared to refractory elements (Kroslakova and Günther 2007, Steenstra *et al.* 2019). Steenstra *et al.* (2019) found also that Cu and Zn behave relatively volatile than refractory during LA-ICP-MS and that matrix effects on laser fractionation are more significant for volatile elements than refractory ones, resulting in substantial inter-laboratory offsets on the analyses of these elements. Regarding element mobility and diffusion to the Pt-Au crucible, Wang *et al.* (2020) performed high temperature and pressure experiments on elemental diffusion from silicate glass to Pt metal and noted that elements like Ni, Cu and Zn are lost at different proportions from the sample through diffusion from the silicate glass to the Pt metal, forming alloys under graphite-buffered conditions (Wang *et al.* 2020). At relatively more oxidizing conditions (FMQ + 2), Cu and Ni are still loss to a great extent, while Zn is not, and at FMQ + 5 only Cu is observed to be lost (Wang *et al.* 2020). Because we did not control fO_2 conditions during glass production in our study, and given that our crucible was not pure Pt, but a PtAu alloy, we can only speculate that these diffusion and migration processes may have also occurred, an assumption that remains

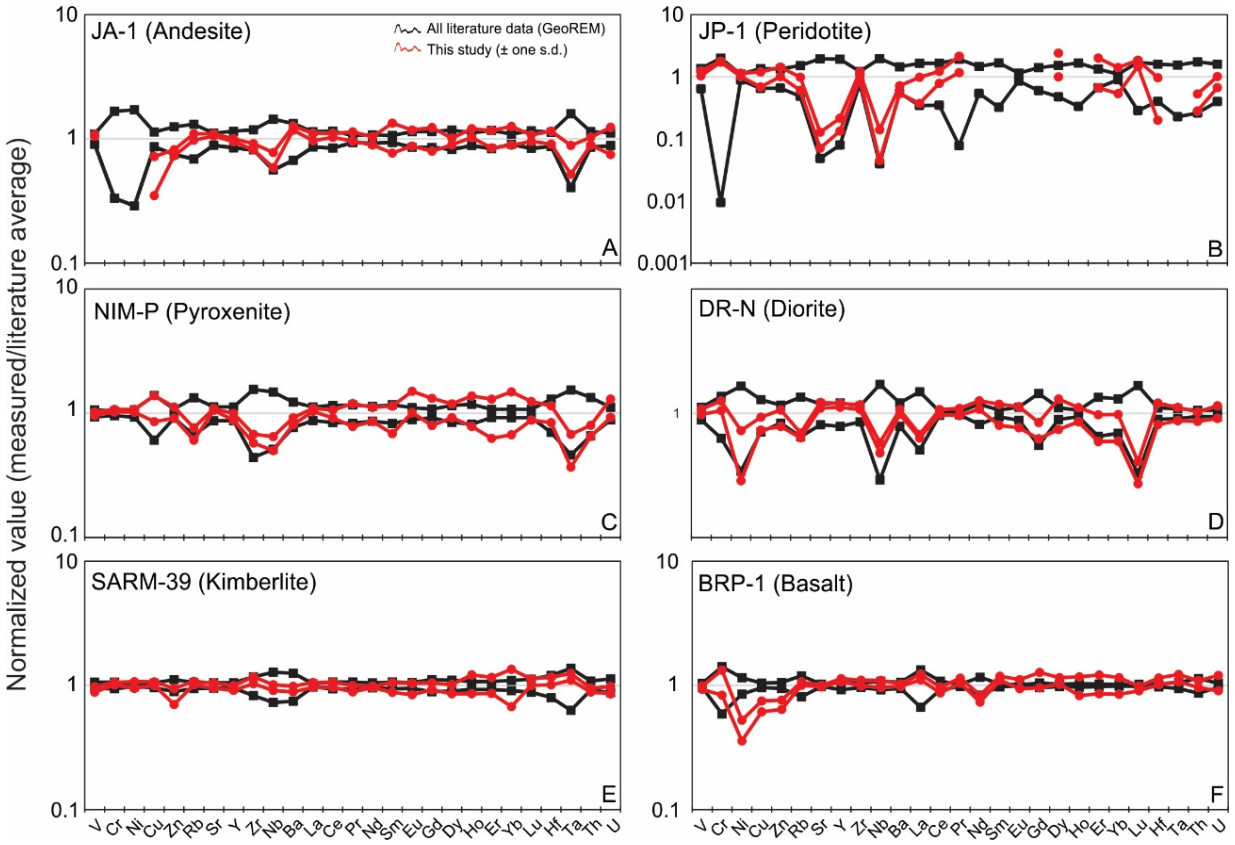

Figure 5. Laser ablation inductively coupled plasma mass spectrometry (LA-ICP-MS) trace element concentration of borosilicate glasses from geological reference materials obtained in this study (*Institut für Mineralogie*, University of Münster) normalized to average values from the literature. Red lines indicate average values plus one standard deviation (minimum and maximum) normalized to the average literature, while black lines are minimum and maximum reported literature data (black lines). Literature data was extracted from the Geological and Environmental Reference Materials database, available at http://georem.mpch-mainz.gwdg.de/ (Jochum *et al.* 2005b).

to be tested. Anyhow, all these fractionation and migration or volatilization effects, when associated, can likely lead to a result divergent than the ones found in literature for elements like Cu, Ni, and Zn, in a similar fashion to the observed in this study, and it is a complex task to individualize each of their effects one by one. It is likely, however, for the reasons stated above, that the depletion observed in Cu, Ni, and Zn was caused either during glass production, by migration or volatilization (e.g., Steenstra *et al.* 2019, Wang *et al.* 2020) rather than due to LIEF (Jenner and Arevalo 2016).

A different approach, instead of considering average, minimum and maximum literature values for the RM as guidelines for method precision and accuracy, is to compare our data with "preferred" values. Preferred values are reported for some RM at the GeoReM, especially those that are widely used in geochemistry laboratories and go through a thorough revision on their trace element content (e.g., Jochum *et al.* 2005a, Jochum *et al.* 2016). For example, Jochum *et al.* (2016) published "preferred" values for the most accessed rock RM samples of the GeoReM database. These authors determined RV and their uncertainties at the 95% confidence level following ISO guidelines and the Certification Protocol of the International Association of Geoanalysts (Kane *et al.* 2003, 2007), and include data obtained by techniques that have different levels of metrological confidence reported in the literature. Given that several methods exist to acquire trace element contents in geological materials, and each one has its own degree of precision and accuracy, Jochum *et al.* (2016) grouped all analytical data for the RM by their metrological properties in decreasing order of confidence, being the primary or definitive values those obtained by isotope dilution using TIMS, MC-ICP-MS and ICP-MS. The authors state that ID-MS data has the highest degree of confidence because operations can be completely described and understood, and for which a complete uncertainty statement can be written (CCQM 1988, Jochum *et al.* 2016). The second and third group divided by Jochum *et al.* (2016) are methods that also have a high-level of confidence, including on the second solution methods such as SN-ICP-MS, ICP-AES and AAS, and on the third XRF, INAA and SSMS, being the difference that the first either uses certified standard solutions of matrix matching RM while in the latter calibration is done mainly on non-certified RM (Jochum *et al.* 2016). Glass beads

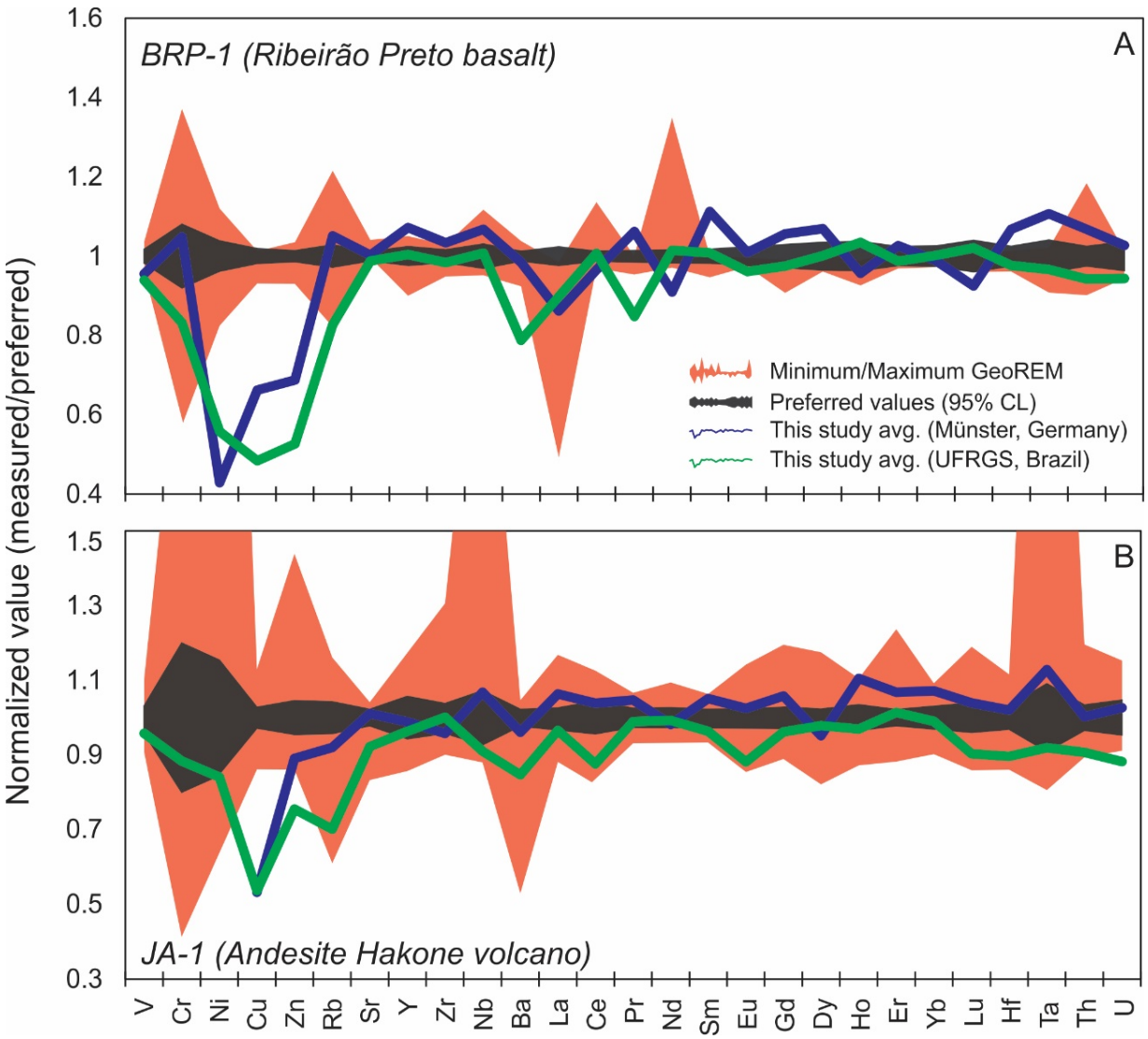

Figure 6. Trace element concentration for geological reference materials (A) BRP-1 and (B) JA-1 obtained in this study normalized to preferred values of Jochum *et al.* (2016) and Cotta and Enzweiler (2008), with comparison of minimum and maximum literature values (Jochum *et al.* 2005b), as well as preferred values at 95% confidence level (Cotta and Enzweiler 2008).

(such as this study) or pressed powder pellets (e.g., Peters and Pettke 2017) are grouped in a fourth category by Jochum *et al.* (2016), having the lowest degree of confidence because of possible inhomogeneities and matrix effects (e.g., Hervig *et al.* 2006, Jochum *et al.* 2014). By collecting data reported for RM from all these methods and carefully analyzing analytical procedures and applying Horwitz function, Jochum *et al.* (2016) assigned a more reliable set of RV to nineteen rock standard RM, including the JA-1 andesite we used in our study.

In our study, two samples have preferred values reported in the GeoReM, the JA-1 (Jochum *et al.* 2016) and the BRP-1 (Cotta and Enzweiler 2008). This allows us to do a more thorough comparison and evaluate quality of our data. In Figure 6, there are average values measured in our study normalized to the preferred values for the JA-1 and BRP-1. When the average value from the data acquired in our study is compared to the preferred values for the BRP-1 basalt and the JA-1 andesite, three elements (Ni, Cu and Zn) have values that deviate more than 15% of the preferred values. This means that all the rest 24 trace elements have average values that lie within ± 15% of the preferred ones (Cotta and Enzweiler 2008, Jochum *et al.* 2016). In any case, the offset of 15% is higher than the standard deviation for several of our analyses and much higher than the standard deviation of the preferred value itself, which normally do not exceed 5%. This is probably due to the generally low precision of the LA-ICP-MS technique when compared to other methods, especially isotope dilution (e.g., Jochum *et al.* 2016). Nevertheless, the precision and accuracy obtained in this study is similar to other studies dealing with LA-ICP-MS (Eggins 2003).

CONCLUSIONS

We presented a method for determining precisely and accurately whole-rock trace element contents using LA-ICP-MS on glass beads produced by mixing high-purity sodium borate and rock powders at high-temperature. By applying this method, values for twenty four refractory litophile trace elements (including LILE, HFSE and REE) in the range of ppb to ppm obtained in six RM in our study are mostly within error from the reported minimum and maximum values in the literature, with an overall agreement of more than 90%. This method has also shown that, in the absence of a matrix-matching standard, the NIST SRM 612 glass can be used as external standards to obtain trace element concentration in silicate materials with an average to good reproducibility. Measured values of Ni, Cu, and Zn were compromised probably due to their siderophile/chalcophile nature or even through their volatile behavior and laser induced element fractionation. This issue will also be observed if we apply this method to analyze trace elements that tend to be volatile, chalcophile or siderophile at magmatic temperatures, such as Ga, Ge, Mo, W, and Pb. Even though in our study laser induced element fractionation seems to not have impact negatively in the results for refractory elements, the use of femtosecond lasers could potentially produce a more robust dataset (e.g., Jochum *et al.* 2014). Moreover, one alternative for the current method would be to analyse via LA-ICP-MS pressed rock powders, which has been proved recently to also be an efficient and clean procedure for the measurement of several trace elements in bulk rock, including those that cannot be measured by the flux melting technique (e.g, Peters and Pettke 2017).

ACKNOWLEDGEMENTS

We acknowledge the technical and scientific staff at the Isotope Geology Laboratory, Instituto de Geociências, Universidade Federal do Rio Grande do Sul (UFRGS) for assistance. The Geological Survey of Japan (GSJ), South African National Mineral Research Organisation (Mintek), Association Nationale de la Recherche et de la Technologie (France) and Instituto de Geociências/UNICAMP (Brazil) are thanked for providing standard RM. This study has received funding from PETROBRAS Science and Technology development program (2017/00216-4). We are also grateful to the three anonymous reviewers and editors C. Riccomini and M. Ibañez-Mejia for their insightful questions, comments and suggestions, which contributed to greatly improve the quality of the manuscript.

ARTICLE INFORMATION

Manuscript ID: 20200057. Received on: 06/30/2020. Approved on: 12/26/2020.

F.P.L.: Conceptualization, Methodology, Analysis, Investigation, Writing, Reviewing, Discussion; A.C.W.: Conceptualization, Methodology, Analysis, Investigation, Writing, Reviewing, Discussion; C.C.P.: Analysis, Investigation, Reviewing, Discussion; N.I.M.V.: Conceptualization, Methodology, Investigation; J.B.: Analysis, Investigation, Reviewing, Discussion; S.K.: Investigation, Reviewing, Discussion; R.V.C.: Conceptualization, Project Funding Acquisition, Investigation, Reviewing, Discussion. F.P.L. and A.C.W. contributed equally as first authors of this study.

Competing interests: The authors declare no competing interests.

REFERENCES

Arevalo, R. Jr. 2014. Laser ablation ICP–MS and laser fluorination GS–MS. *In*: Holland H.D., Turekian K.K. (Eds). *Treatise on Geochemistry*. 2nd Ed. Oxford: Elsevier, p. 425-441.

CCQM. 1988. *Minutes from the fifth meeting of the Consultative Committee on the Quantity of Material (CCQM) of the Bureau International des Poids et Mesures (BIPM)*. Sévres, France: CCQM.

Chen Z. 1999. Inter-element fractionation and correction in laser ablation inductively coupled plasma mass spectrometry. *Journal of Analytical Atomic Spectrometry*, **14**(12):1823-1828.

Cotta A.J.B., Enzweiler J. 2008. Certificate of Analysis of the Reference Material BRP-1 (Basalt Ribeirão Preto). *Geostandards and Geoanalytical Research*, **32**(2):231-235. https://doi.org/10.1111/j.1751-908X.2008.00894.x

DesOrmeau J.W., Gordon S.M., Kylander-Clark A.R.C., Hacker B., Bowring A., Schoene B., Samperton K.M. 2015. Insights into (U)HP metamorphism of the Western Gneiss Region, Norway: A high-spatial resolution and high-precision zircon study. *Chemical Geology*, **414**:138-155. https://doi.org/10.1016/j.chemgeo.2015.08.004

Eggins S.M. 2003. Laser ablation ICP-MS analysis of geological materials prepared as lithium borate glasses. *Geostandards Newsletter*, **27**(2):147-162. https://doi.org/10.1111/j.1751-908X.2003.tb00642.x

Eggins S.M., Kinsley L.P.J., Shelley J.M.G. 1998. Deposition and element fractionation processes during atmospheric pressure laser sampling for analysis by ICP-MS. *Applied Surface Science*, **127-129**:278-286. https://doi.org/10.1016/S0169-4332(97)00643-0

Fisher C.M., Bauer A.M., Luo Y., Sarkar C., Hanchar J.M., Vervoort J.D., Tapster S.R., Horstwood M., Graham Pearson D. 2020. Laser ablation split-stream analysis of the Sm-Nd and U-Pb isotope compositions of monazite, titanite, and apatite – Improvements, potential reference materials, and application to the Archean Saglek Block gneisses. *Chemical Geology*, **539**:119493. https://doi.org/10.1016/j.chemgeo.2020.119493

Fryer B.J., Jackson S.E., Longerich H.P. 1995. The design, operation and role of the laser-ablation microprobe coupled with an inductively coupled plasma – mass spectrometer (LAM–ICP–MS) in the Earth sciences. *Canadian Mineralogist*, **33**(2):303-312.

Gaboardi M., Humayun M. 2009. Elemental fractionation during LA-ICP-MS analysis of silicate glasses: implications for matrix-independent standardization. *Journal of Analytical Atomic Spectrometry*, **24**(9):1188-1197. https://doi.org/10.1039/B900876D

Golitko M. 2016. *Recent Advances in Laser Ablation ICP-MS for Archaeology*. Verlag, Berlin: Springer, 358 p.

Gray A.L. 1985. Solid sample introduction by laser ablation for inductively coupled plasma source mass spectrometry. *Analyst*, **110**:551-556. https://doi.org/10.1039/AN9851000551

Griffin W.L., Powell W.J., Pearson N.J., O'Reilly S.Y. 2008. Glitter: Data reduction software for laser ablation ICP-MS. *In*: Sylvester P.J. (ed.). *Laser Ablation ICP-MS in the Earth Sciences:* Current Practices and Outstanding Issues, Mineralogical Association of Canada Short Course Series, Short Course 40. Vancouver, B.C.: Mineralogical Association of Canada, p. 308-311.

Guillong M., Horn I., Günther D. 2003. A comparison of 266 nm, 213 nm and 193 nm produced from a single solid state Nd:YAG laser for laser ablation ICP-MS. *Journal of Analytical Atomic Spectrometry*, **18**(10):1224-1230. https://doi.org/10.1039/B305434A

Günther D., von Quadt A., Wirz R., Cousin H., Dietrich V.J. 2001. Elemental analysis using laser ablation-inductively coupled plasma-mass spectrometry (LA-ICP-MS) of geological samples fused with $Li_2B_4O_7$ and calibrated without matrix-matched standards. *Mikrochimica Acta*, **136**:101-107. https://doi.org/10.1007/s006040170038

Hergenröder R. 2006. A model of non-congruent laser ablation as a source of fractionation effects in LA-ICP-MS. *Journal of Analytical Atomic Spectrometry*, **21**(5):505-516. https://doi.org/10.1039/B600698A

Hervig R.L., Mazdab F.K., Williams P., Guan Y., Huss G.R., Leshin L.A. 2006. Useful ion yields for Cameca IMS 3f and 6f SIMS: Limits on quantitative analysis. *Chemical Geology*, **227**(1-2):83-99. https://doi.org/10.1016/j.chemgeo.2005.09.008

Horn I., von Blanckenburg F. 2007. Investigation on elemental and isotopic fractionation during 196 nm femtosecond laser ablation multiple collector inductively coupled plasma mass spectrometry. *Spectrochimica Acta - Part B Atomic Spectroscopy*, **62**(4):410-422. https://doi.org/10.1016/j.sab.2007.03.034

Hutchinson D., McDonald I. 2008. Laser ablation ICP-MS study of platinum-group elements in sulphides from the Platreef at Turfspruit, northern limb of the Bushveld Complex, South Africa. *Mineralium Deposita*, **43**:695-711. https://doi.org/10.1007/s00126-008-0190-6

Ingamells C.O. 1970. Lithium metaborate flux in silicate analysis. *Analytica Chimica Acta*, **52**(2):323-334. https://doi.org/10.1016/S0003-2670(01)80963-6

Jackson S.E. 2008. Calibration strategies for elemental analysis by LA–ICP–MS. *In*: Sylvester P. (ed.). *Laser Ablation ICP–MS in the Earth Sciences:* Current Practices and Outstanding Issues. Mineralogical Association of Canada Short Course. Vancouver: Mineralogical Association of Canada, p. 169-188.

Jackson S.E., Longerich H.P., Dunning G.R., Fryer B.J. 1992. The application of laser-ablation microprobe – inductively coupled plasma – mass spectrometry (LAM-ICP-MS) to in situ trace-element determinations in minerals. *Canadian Mineralogist*, **30**(4):1049-1064.

Jenner F., Arevalo Jr. R.D. 2016. Major and Trace Element Analysis of Natural and Experimental Igneous Systems using LA–ICP–MS. *Elements*, **12**(5):311-316. https://doi.org/10.2113/gselements.12.5.311

Jenner F.E., O'Neill H.St.C. 2012. Analysis of 60 elements in 616 ocean floor basaltic glasses. *Geochemistry, Geophysics, Geosystems*, **13**(2). https://doi.org/10.1029/2011GC004009

Jochum K.P., Nohl U., Herwig K., Lammel E., Stoll B., Hofmann A.W. 2005b. GEOREM: A new geochemical database for reference materials and isotopic standards. *Geostandards and Geoanalytical Research*, **29**(3):333-338. https://doi.org/10.1111/j.1751-908X.2005.tb00904.x

Jochum K.P., Scholz D., Stoll B., Weis U., Wilson S.A., Yang Q., Schwalb A., Börner N., Jacob D.E., Andreae M.O. 2012. Accurate trace element analysis of speleothems and biogenic calcium carbonates by LA-ICP-MS. *Chemical Geology*, **318-319**:31-44. https://doi.org/10.1016/j.chemgeo.2012.05.009

Jochum K.P., Stoll B., Pfänder J.A., Seufert M., Flanz M., Maissenbacher P., Hofmann M., Hofmann A.W. 2001. Progress in multi-ion counting spark-source mass spectrometry (MIC-SSMS) for the analysis of geological samples. *Fresenius' Journal of Analytical Chemistry*, **370**:647-653. https://doi.org/10.1007/s002160100786

Jochum K.P., Stoll B., Weis U., Jacob D.E., Mertz-Kraus R., Andrea M.O. 2014. Non-Matrix-Matched Calibration for the Multi-Element Analysis of Geological and Environmental Samples Using 200 nm Femtosecond LA-ICP-MS: A Comparison with Nanosecond Lasers. *Geostandards and Geoanalytical Research*, **38**(3):265-292. https://doi.org/10.1111/j.1751-908X.2014.12028.x

Jochum K.P., Weis U., Schwager B., Stoll B., Wilson S.A., Haug G.H., Andreae M.O., Enzweiler J. 2016. Reference Values Following ISO Guidelines for Frequently Requested Rock Reference Materials. *Geostandards and Geoanalytical Research*, **40**(3):333-350. https://doi.org/10.1111/j.1751-908X.2015.00392.x

Jochum K.P., Weis U., Stoll B., Kuzmin D., Yang Q., Raczek I., Jacob D.E., Stracke A., Birbaum K., Frick D.A., Günther D., Enzweiler J. 2011. Determination of Reference Values for NIST SRM 610–617 Glasses Following ISO Guidelines. *Geostandards and Geoanalytical Research*, **35**(4):397-429. https://doi.org/10.1111/j.1751-908X.2011.00120.x

Jochum K.P., Willbold M., Raczek I., Stoll B., Herwig K. 2005a. Chemical Characterisation of the USGS Reference Glasses GSA-1G, GSC-1G, GSD-1G, GSE-1G, BCR-2G, BHVO-2G and BIR-1G Using EPMA, ID-TIMS, ID-ICP-MS and LA-ICP-MS. *Geostandards and Geoanalytical Research*, **29**(3):285-302. https://doi.org/10.1111/j.1751-908X.2005.tb00901.x

Kane J.S., Potts P.J., Meisel T., Wiedenbeck M. 2007. International Association of Geoanalysts' protocol for the certification of geological and environmental reference materials: A supplement. *Geostandards and Geoanalytical Research*, **31**(3):285-288. https://doi.org/10.1111/j.1751-908X.2007.00869.x

Kane J.S., Potts P.J., Wiedenbeck M., Carignan J., Wilson S. 2003. International Association of Geoanalysts' protocol for the certification of geological and environmental reference materials. *Geostandards Newsletter: Journal of Geostandards and Geoanalysis*, **27**(3):227-244. https://doi.org/10.1111/j.1751-908X.2003.tb00724.x

Kelemen P.B., Shimizu N., Dunn T. 1993. Relative depletion of niobium in some arc magmas and the continental crust: partitioning of K, Nb, La and Ce during melt/rock reaction in the upper mantle. *Earth and Planetary Science Letters*, **120**(3-4):111-134. https://doi.org/10.1016/0012-821X(93)90234-Z

Kempenaers L., Janssens K., Jochum K.P., Vincze L., Vekemans B., Somogyi A., Drakopoulos M., Adams F. 2003. Micro-heterogeneity study of trace elements in USGS, MPI-DING and NIST glass reference materials by means of synchrotron micro-XRF. *Journal of Analytical Atomic Spectrometry*, **18**(4):350-357. https://doi.org/10.1039/B212196D

Kylander-Clark A., Hacker B., Cottle J. 2013. Laser Ablation Split-Stream ICP Petrochronology. *Chemical Geology*, **345**:99-112. https://doi.org/10.1016/j.chemgeo.2013.02.019

Koch J., Feldmann I., Jakubowski N., Niemax K. 2002. Elemental composition of laser ablation aerosol particles deposited in the transport tube to an ICP. *Spectrochimica Acta part B*, **57**(5):975-985. https://doi.org/10.1016/S0584-8547(02)00021-6

Korotev R.L. 1996. A self-consistent compilation of elemental concentration data for 93 geochemical reference samples. *Geostandards Newsletter*, **20**(2):217-245. https://doi.org/10.1111/j.1751-908X.1996.tb00185.x

Kosler J., Wiedenbeck M., Wirth R., Hovorka J., Sylvester P., Míková J. 2005. Chemical and phase composition of particles produced by laser ablation of silicate glass and zircon—implications for elemental fractionation during ICP-MS analysis. *Journal of Analytical Atomic Spectrometry*, **20**:402-409. https://doi.org/10.1039/B416269B

Kroslakova I., Günther D. 2007. Elemental fractionation in laser ablation-inductively coupled plasma-mass spectrometry: evidence for mass load induced matrix effects in the ICP during ablation of a silicate glass. *Journal of Analytical Atomic Spectrometry*, **22**:51-62. https://doi.org/10.1039/B606522H

Kuhn H.R., Günther D. 2004. Laser ablation-ICP-MS: particle size dependent elemental composition studies on filter-collected and online measured aerosols from glass. *Journal of Analytical Atomic Spectrometry*, **19**:1158-1164. https://doi.org/10.1039/B404729J

Leitzke F.P., Fonseca R.O.C., Sprung P., Mallmann G., Lagos M., Michely L.T., Münker C. 2017. Redox dependent behaviour of molybdenum during magmatic processes in the terrestrial and lunar mantle: Implications for the Mo/W of the bulk silicate Moon. *Earth and Planetary Science Letters*, **474**:503-515. https://doi.org/10.1016/j.epsl.2017.07.009

Lodders K. 2003. Solar system abundances and condensation temperatures of the elements. *The Astrophysical Journal*, **591**(2):1220-1247. https://doi.org/10.1086/375492

Longerich H. 2008. Laser ablation–inductively coupled plasma mass spectrometry (LA-ICPMS). *In*: Sylvester P.J. (ed.). *Laser Ablation ICP-MS in the Earth Sciences:* Current practice and outstanding issues. Short Course Series Mineralogical Association of Canada. Vancouver: Mineralogical Association of Canada, p. 11-18.

Longerich H.P., Jackson S.E., Günther D. 1996. Laser ablation inductively coupled plasma mass spectrometric transient signal data acquisition and analyte concentration calculation. *Journal of Analytical Atomic Spectrometry*, **11**:899-904. https://doi.org/10.1039/JA9961100899

Mahan B., Siebert J., Pringle E.A., Moynier F. 2017. Elemental partitioning and isotopic fractionation of Zn between metal and silicate and geochemical estimation of the S content of the Earth's core. *Geochimica et Cosmochimica Acta*, **196**:252-270. https://doi.org/10.1016/j.gca.2016.09.013

Münker C. 2010. A high field strength element perspective on early lunar differentiation. *Geochimica et Cosmochimica Acta*, **74**(24):7340-7361. https://doi.org/10.1016/j.gca.2010.09.021

Nesbitt R.W., Hirata T., Butler I.B., Milton J.A. 1997. UV laser ablation ICP-MS: Some applications in the Earth sciences. *Geostandards Newsletter*, **21**(2):231-243. https://doi.org/10.1111/j.1751-908X.1997.tb00943.x

Ødegård M., Hamester M. 1997. Preliminary investigation into the use of a high resolution inductively coupled plasma-mass spectrometer with laser ablation for the analysis of geological material fused with $Li_2B_4O_7$. *Geostandards Newsletter*, **21**(2):245-252. https://doi.org/10.1111/j.1751-908X.1997.tb00673.x

Outridge P.M., Doherty W., Gregoire D.C. 1998. Determination of trace elemental signatures in placer gold by laser ablation–inductively coupled plasma–mass spectrometry as a potential aid for gold exploration. *Journal of Geochemical Exploration*, **60**(3):229-240. https://doi.org/10.1016/S0375-6742(97)00049-6

Palme H., O'Neill H.S.C. 2014. Cosmochemical estimates of mantle composition. *Treatise on Geochemistry*, **3**:1-39. https://doi.org/10.1016/B978-0-08-095975-7.00201-1

Panteeva S.V., Gladkochoub D.P., Donskaya T.V., Markova V.V., Sandimirova G.P. 2003. Determination of 24 trace elements in felsic rocks by inductively coupled plasma-mass spectrometry after lithium metaborate fusion. *Spectrochimica Acta Part B*, **58**(2):341-350. https://doi.org/10.1016/S0584-8547(02)00151-9

Pearce J.A., Gale G.H. 1977. Identification of ore deposition environments from trace element geochemistry of associated igneous host rocks. *Geological Society*, **7**(1):14-24. https://doi.org/10.1144/GSL.SP.1977.007.01.03

Pearce J.A., Harris N.B.W, Tindle A.G. 1984. Trace element discrimination diagrams for the tectonic interpretation of granitic rocks. *Journal of Petrology*, **25**(4):956-983. https://doi.org/10.1093/petrology/25.4.956

Perkins, W.T., Pearce, N.J.G., Jeffries, T.E. 1993. Laser ablation inductively coupled plasma mass spectrometry: A new technique for the determination of trace and ultra-trace elements in silicates. *Geochimica et Cosmochimica Acta*, **57**(2):475-482. https://doi.org/10.1016/0016-7037(93)90447-5

Peters D., Pettke T. 2017. Evaluation of Major to Ultra Trace Element Bulk Rock Chemical Analysis of Nanoparticulate Pressed Powder Pellets by LA-ICP-MS. *Geostandards and Geoanalytical Research*, **41**(1):5-28. https://doi.org/10.1111/ggr.12125

Pfänder J.A., Münker C., Stracke A., Mezger K. 2007. Nb/Ta and Zr/Hf in ocean island basalts: Implications for crust–mantle differentiation and the fate of Niobium. *Earth and Planetary Science Letters*, **254**(1-2):158-172. https://doi.org/10.1016/j.epsl.2006.11.027

Pinto F.G., Escalfoni-Junior R., Saint'Pierre T.D. 2012. Sample Preparation for Determination of Rare Earth Elements in Geological Samples by ICP-MS: A Critical Review. *Analytical Letters*, **45**(12):1537-1556. https://doi.org/10.1080/00032719.2012.677778

Potts P.J. 1992. *A handbook of silicate rock analysis*. United States: Springer, 622 p.

Reich M., Simon A.C., Deditius A., Barra F., Chryssoulis S., Lagas G., Tardani D., Knipping J., Bilenker L., Sánchez-Alfaro P., Roberts M.P., Munizaga R. 2016. Trace element signature of Pyrite from the Los Colorados iron oxide-apatite (IOA) deposit, Chile: A missing link between andean IOA and iron oxide copper-gold systems? *Economic Geology*, **111**(3):743-761. https://doi.org/10.2113/econgeo.111.3.743

Rocholl A. 1998. Major and Trace Element Composition and Homogeneity of Microbeam Reference Material: Basalt Glass USGS BCR-2G. *Geostandards and Geoanalytical Research*, **22**(1):33-45. https://doi.org/10.1111/j.1751-908X.1998.tb00543.x

Russo R.E., Mao X., Gonzalez J.J., Zorba V., Yoo J. 2013. Laser ablation in analytical chemistry. *Analytical Chemistry*, **85**(13):6162-6177. https://doi.org/10.1021/ac4005327

Siebert J., Corgne A., Ryerson F.J. 2011. Systematics of metal–silicate partitioning for many siderophile elements applied to Earth's core formation. *Geochimica et Cosmochimica Acta*, **75**(6):1451-1489. https://doi.org/10.1016/j.gca.2010.12.013

Steenstra E.S., Berndt J., Klemme S., van Westrenen W. 2019. LA-ICP-MS analyses of Fe-rich alloys: quantification of matrix effects for 193 nm excimer laser systems. *Journal of Analytical Atomic Spectrometry*, **34**(1):222-231. https://doi.org/10.1039/C8JA00291F

Taylor V.F., Toms A., Longerich H.P. 2002. Acid digestion of geological and environmental samples using open-vessel focused microwave digestion. *Analytical and Bioanalytical Chemistry*, **372**:360-365. https://doi.org/10.1007/s00216-001-1172-z

Tomascak P.B., Magna T., Dohmen R. 2012. *Advances in lithium isotope geochemistry*. Berlin: Springer, 195 p.

Van Achterbergh E., Ryan C.G., Jackson S.E., Griffin W.L. 2001. Data reduction software for LA-ICP-MS: appendix. *In*: Sylvester P.J. (ed.), *Laser Ablation–ICP-Mass Spectrometry in the Earth Sciences:* Principles and Applications. Mineralogical Association of Canada Short Course Series. Ottawa: Mineralogical Association of Canada, v. 29, p. 239-243.

Wang J., Xiong X., Zhang L., Takahashi E. 2020. Element loss to platinum capsules in high-temperature–pressure experiments. *American Mineralogist*, **105**(10):1593-1597. https://doi.org/10.2138/am-2020-7580

Whalen J.B., Currie K.L., Chappell B.W. 1987. A-type granites: geochemical characteristics, discrimination and petrogenesis. *Contributions to Mineralogy and Petrology*, **95**:407-419. https://doi.org/10.1007/BF00402202

White W.M. 2013. *Geochemistry*. Hoboken: Wiley Blackwell, 660 p.

Wu S., Karius V., Schmidt B.C., Simon K., Wörner G. 2018. Comparison of Ultrafine Powder Pellet and Flux-free Fusion Glass for Bulk Analysis of Granitoids by Laser Ablation-Inductively Coupled Plasma-Mass Spectrometry. *Geostandards and Geoanalytical Research*, **42**(4):575-591. https://doi.org/10.1111/ggr.12230